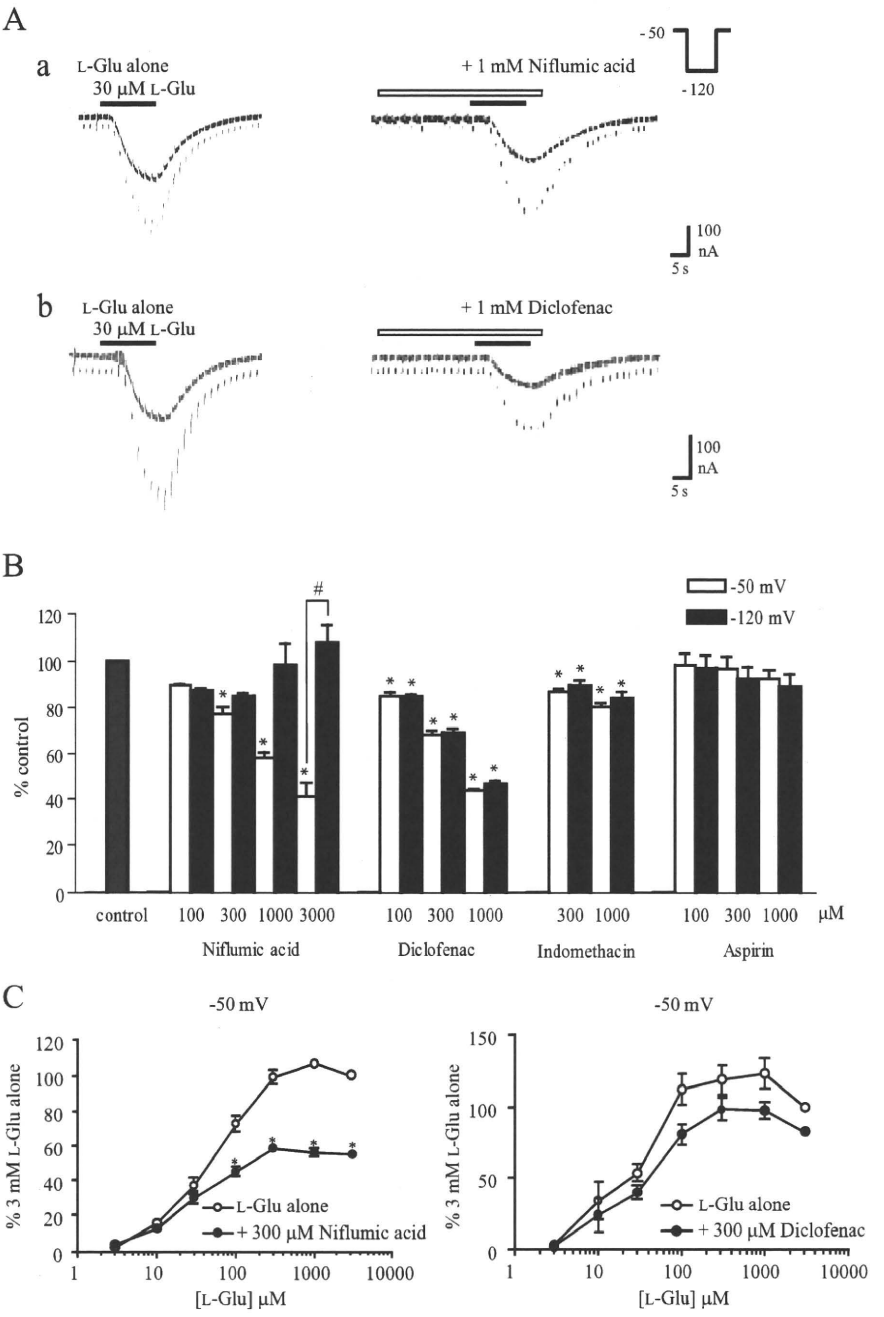

Fig. 1. Effects of NFA and diclofenac on L-Glu-induced currents in EAAT1-expressing *Xenopus* oocytes. A: The traces of L-Glu (30 μM)–induced inward currents in the presence or the absence of NFA (a) or diclofenac (b) at −50 mV (bold line) and −120 mV (thin line). The oocytes were held at −50 mV and hyperpolarized to −120 mV for 400 ms, every 2 s. B: Concentration–response relationships for various NSAIDs at −50 and −120 mV. The amplitude of EAAT1 current in the presence of the drug was normalized to that just before the application. NFA (n = 5 – 9), diclofenac (n = 5), and indomethacin (n = 5) significantly inhibited EAAT1 currents. Aspirin (n = 4) did not affect EAAT1 currents. The inhibition by NFA was always more remarkable at −50 mV than at −120 mV. $^{*}P < 0.05$ vs. the control group. $^{\#}P < 0.05$ vs. the −50 mV group. Tukey's test following ANOVA. C: Concentration–response curves of EAAT1 currents at −50 mV in the absence or the presence of NFA (n = 9) (left) or diclofenac (n = 8) (right). The currents were normalized to the maximal current induced by 3 mM L-Glu. I_{max} and $K_{0.5}$ were calculated using every concentration–response trace by fitting with the following equation: $I = I_{max}[\text{L-Glu}] / (K_{0.5} + [\text{L-Glu}])$, using Graphpad PRISM 4 for Windows. Mean I_{max} with the drug was normalized to the mean I_{max} without drug. Treatment with NFA (n = 9) and diclofenac (n = 8) resulted in a decrease in the I_{max} without affecting the $K_{0.5}$ (Student's *t*-test). $^{*}P < 0.05$ vs. the control group. Tukey's test following ANOVA.

transient outward current varied by Cl^-. Although NFA is reported to inhibit CaCC (6), the contribution of CaCC to EAAT1 current may be negligible at −50 and −120 mV according to the report. Diclofenac (100 μM – 1 mM) inhibited the EAAT1 current dose-dependently. Indomethacin (100 and 300 μM) inhibited the EAAT1 current, but the effects were even weaker. In the case of diclofenac and indomethacin, the strength of the effects at −50 and −120 mV were almost the same. Aspirin (100 μM – 1 mM) had no effects. At −50 mV, co-application of NFA with varying doses of L-Glu significantly reduced the maximal current (I_{max}) to 55.1 ± 1.8% (Fig. 1C, left). The affinity for L-Glu ($K_{0.5}$) was not affected by NFA (from 50.0 ± 5.0 to 33.9 ± 6.3 μM). Similarly, diclofenac resulted in a decrease in the I_{max} (81.7 ± 1.2%) without affecting the $K_{0.5}$ (from 27.3 ± 4.0 to 35.2 ± 6.3 μM) in a non-competitive manner (Fig. 1C, right). Although vehicle alone had no significant effect on I_{max} and $K_{0.5}$ (data not shown), the $K_{0.5}$ value for diclofenac-vehicle was smaller than that for NFA-vehicle, which might have been attributed to the slight conformational change caused by DMSO and MeOH. Taken together, these results suggest that NFA and diclofenac modulate EAAT1 via a site different from the L-Glu recognition site.

AA is known to decrease EAAT1 current in a noncompetitive manner (7). Therefore, we compared the effects of NFA and diclofenac when co-applied with AA. The doses used for NFA and diclofenac were determined so as to obtain the equivalent effects and not to reach maximum effects (Fig. S1) (Supplementary Figure: available in the online version only). NFA and AA have an almost additive effect (Fig. 2A). Diclofenac and AA did not show an additive effect (Fig. 2B). The enhancement by AA of diclofenac's effect was significantly weaker than that of NFA's effect (Fig. 2C). These results imply that NFA and diclofenac interact with EAAT1 in different manners.

Figure 3A shows representative current–voltage curves for the EAAT1 currents in the presence or in the absence of NFA. The current value in the presence of NFA alone has been subtracted from that in the presence of NFA and L-Glu. NFA produced a significant leftward shift of reversal potential (E_{rev}) (from 28.9 ± 5.1 to 5.2 ± 5.7 mV). At the potentials more negative than −100 mV, NFA increased the current amplitude. The influence of NFA on the current amplitude was voltage-dependent (Fig. 3B). Diclofenac inhibited the current amplitude to the same extent at all negative potentials and had no effects on the E_{rev} (from 33.8 ± 9.1 to 27.5 ± 6.1 mV) (Fig. 3: C and D). These results further support the implication that NFA and diclofenac interact with EAAT1 in different manners.

The differences in voltage dependency and the effects

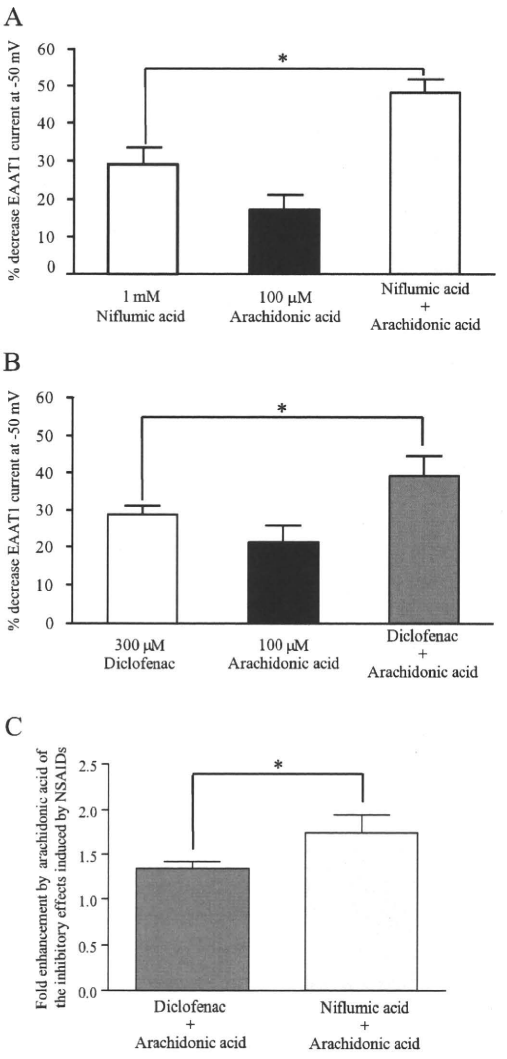

Fig. 2. AA differently influenced the effects of NFA and diclofenac. A and B: The percentage decrease was calculated by comparing the current amplitude induced by 30 μM L-Glu with drugs to that induced by L-Glu alone at −50 mV. NFA and AA have an almost additive effect (28.9 ± 4.6% decrease for NFA [1 mM], 17.4 ± 3.8% decrease for AA [100 μM], 48.3 ± 3.4% decrease for NFA + AA, n = 4). Although AA also enhanced the inhibitory effect of diclofenac, the enhancement was even weaker than that of NFA (28.7 ± 2.6% decrease for diclofenac [300 μM], 21.3 ± 4.3% decrease for AA [100 μM], 39.3 ± 4.0% decrease for diclofenac + AA, n = 5). *$P < 0.05$ vs. the NSAIDs alone group. Paired t-test. C: The fold enhancement was calculated by comparing the percentage decrease by NSAIDs to that by NSAIDs with AA at −50 mV. The enhancement by AA of diclofenac's effects was significantly weaker than that of NFA's effect (1.7 ± 0.2 vs. 1.3 ± 0.1 fold; *$P < 0.05$, Student's t-test).

on E_{rev} suggest that NFA and diclofenac regulate EAAT1 via different mechanisms. The EAAT1 currents are the net result of charge movements from amino acid (aa) and ion cotransport (Na^+ / H^+ / K^+) (I_{aa}) and the ligand-gated Cl^- conductance (I_{Cl}) (8). NFA has been reported to en-

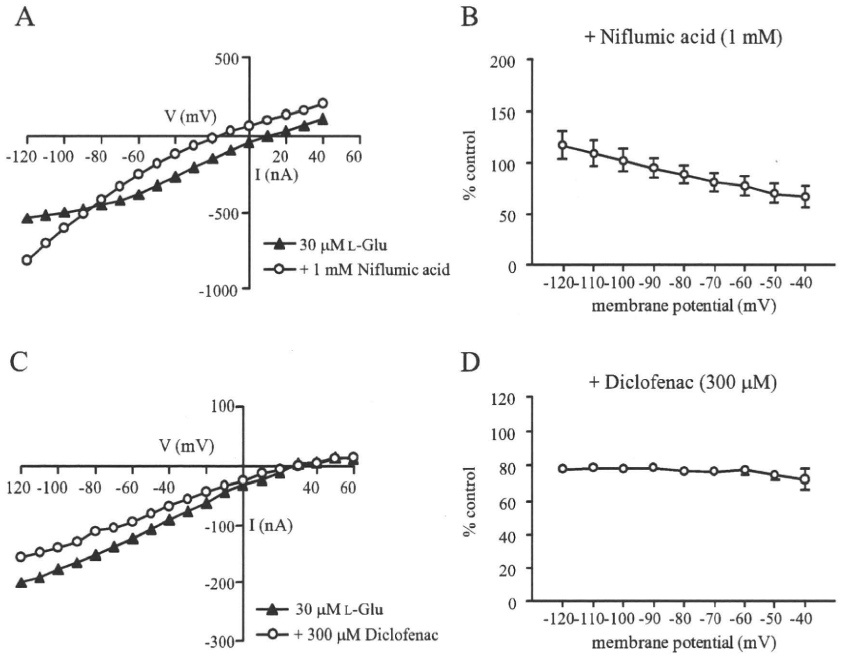

Fig. 3. The effect of NFA is voltage-dependent. A and C: Representative current–voltage relations for 30 μM L-Glu in the presence or the absence of 1 mM NFA (A) and 300 μM diclofenac (C). The current–voltage relationships were obtained with a holding potential of −50 mV and implementing 400-ms voltage jumps in 10-mV increments over the range from −120 to +60 mV. In the control, current values at steady-state have been subtracted from that in the presence of L-Glu. In the drug (NFA or diclofenac)–treated group, the current value in the presence of drug alone has been subtracted from that in the presence of the drug and L-Glu. NFA (n = 10) produced a leftward shift of E_{rev} ($P < 0.05$), whereas diclofenac (n = 4) had no effect (paired t-test). B and D: The relationship between the effects and the holding potential. The current in the presence of these drugs was normalized to that obtained just before the application. The effect of NFA (n = 10) was voltage-dependent. Diclofenac (n = 5) inhibited the current amplitude to the same extent at all negative potentials.

hance the L-Glu-induced EAAT4 current by activating an uncoupled H^+ conductance (5). In our preliminary data, NFA did not cause a modulation in the rate of I_{aa} and I_{Cl}, but rather modulates an uncoupled H^+ conductance of EAAT1 (unpublished observation), which may be related to the effect of NFA obtained in our study. In contrast, diclofenac altered only the current amplitude but not the E_{rev}. E_{rev} for the net current depends on the relative magnitude of I_{aa} and I_{Cl} (8). Diclofenac might have affected both I_{aa} and I_{Cl} so as not to change E_{rev}. The mechanism for the effects of diclofenac needs further investigation.

In our study, the influences on EAAT1 currents were caused by NFA, diclofenac, and indomethacin but not by aspirin. Mefenamic acid, diclofenac, and indomethacin are known to induce reproducible symptoms in patients with affective disorder (9). Aspirin has not been reported to have such side defects to date. If you take into account that GLAST (rodent EAAT1)–deficient mice showed phenotypic abnormalities related to schizophrenia (10), our results suggest that the psychiatric side effects of some NSAIDs have correlation with their effects on L-Glu transporters. Because NSAIDs have high affinity with the plasma protein, their brain delivery is restricted by the blood brain barrier (11). For example, the concentration of enantiomers of ibuprofen in cerebrospinal fluid is less than 1.5 μM after therapeutic application (12). Based on these data, the effective concentrations of NFA and diclofenac in our study are higher than that expected for therapeutic application. Habjan et al. recently indicated that EAAT1 current was inhibited by NFA. The extent of the effects was application time–dependent and partially irreversible (4), raising the possibility that NFA and diclofenac modulate EAAT1 after long-term administration.

NSAIDs are widely used for patients with inflammation, fever, and pain. Our results may help understanding the mechanisms of side effects caused by some NSAIDs.

Acknowledgments

We thank Dr. Yasuda-Kamatani and Dr. Shimamoto for providing the cDNA of EAAT1 and Dr. Nakagawa and Dr. Shigeri for helpful suggestions. This work was partly supported by a Grant-in-Aid for Young Scientists from MEXT, Japan (KAKENHI 18700373, 21700422); a Grant for Research on Publicly Essential Drugs and Medical Devices from JHSF; and a Health and Labor Science Research Grant for Research on Risks of Chemicals from MHLW, Japan, awarded to K.S.

References

1 Beart PM, O'Shea RD. Transporters for L-glutamate: an update on their molecular pharmacology and pathological involvement. Br J Pharmacol. 2007;150:5–17.
2 Wahner AD, Bronstein JM, Bordelon YM, Ritz B. Nonsteroidal anti-inflammatory drugs may protect against Parkinson disease. Neurology. 2007;69:1836–1842.
3 Browning CH. Nonsteroidal anti-inflammatory drugs and severe psychiatric side effects. Int J Psychiatry Med. 1996;26:25–34.
4 Habjan S, Vandenberg RJ. Modulation of glutamate and glycine

transporters by niflumic, flufenamic and mefenamic acids. Neurochem Res. 2009;34:1738–1747.
5 Poulsen MV, Vandenberg RJ. Niflumic acid modulates uncoupled substrate-gated conductances in the human glutamate transporter EAAT4. J Physiol. 2001;534:159–167.
6 White MM, Aylwin M. Niflumic and flufenamic acids are potent reversible blockers of Ca^{2+}-activated Cl^- channels in Xenopus oocytes. Mol Pharmacol. 1990;37:720–724.
7 Zerangue N, Arriza JL, Amara SG, Kavanaugh MP. Differential modulation of human glutamate transporter subtypes by arachidonic acid. J Biol Chem. 1995;270:6433–6435.
8 Wadiche JI, Amara SG, Kavanaugh MP. Ion fluxes associated with excitatory amino acid transport. Neuron. 1995;15:721–728.
9 Jiang HK, Chang DM. Non-steroidal anti-inflammatory drugs with adverse psychiatric reactions: five case reports. Clin Rheumatol. 1999;18:339–345.
10 Karlsson RM, Tanaka K, Saksida LM, Bussey TJ, Heilig M, Holmes A. Assessment of glutamate transporter GLAST (EAAT1)-deficient mice for phenotypes relevant to the negative and executive/cognitive symptoms of schizophrenia. Neuropsychopharmacology. 2009;34:1578–1589.
11 Parepally JM, Mandula H, Smith QR. Brain uptake of nonsteroidal anti-inflammatory drugs: ibuprofen, flurbiprofen, and indomethacin. Pharm Res. 2006;23:873–881.
12 Bannwarth B, Lapicque F, Pehourcq F, Gillet P, Schaeverbeke T, Laborde C, et al. Stereoselective disposition of ibuprofen enantiomers in human cerebrospinal fluid. Br J Clin Pharmacol. 1995;40:266–269.

Biochemical and Biophysical Research Communications 403 (2010) 138–143

Contents lists available at ScienceDirect

Biochemical and Biophysical Research Communications

journal homepage: www.elsevier.com/locate/ybbrc

Nicotine increases cancer stem cell population in MCF-7 cells

Naoya Hirata, Yuko Sekino, Yasunari Kanda *

Division of Pharmacology, National Institute of Health Sciences, Setagaya 158-8501, Japan

ARTICLE INFO

Article history:
Received 28 October 2010
Available online 3 November 2010

Keywords:
ALDH
Cancer stem cells
Cigarette smoking
Nicotine
Notch
PKC

ABSTRACT

Epidemiological studies have suggested that cigarette smoking is related to increased breast cancer risk. Nicotine is most likely related to the risk in cigarette smoking. However, the mechanisms by which nicotine promotes cancer development are not fully understood. It has recently been suggested that development of breast cancer are originated from cancer stem cells, which are a minor population of breast cancer. In the present study, we investigated the effects of nicotine on the population of cancer stem cells in MCF-7 human breast cancer cells, using flow cytometry with a cancer stem cell marker aldehyde dehydrogenase (ALDH). We found that nicotine increased ALDH-positive cell population in a dose-dependent manner. We further demonstrated that a PKC-Notch pathway is involved in the effect of nicotine. In addition, the effect of nicotine was blocked by treatment with the α7 subunit-selective antagonist of nicotinic acetylcholine receptors (nAChR) α-Bungarotoxin. These data suggest that nicotine increases the stem cell population via α7-nAChR and the PKC-Notch dependent pathway in MCF-7 cells. These findings reveal a relationship between nicotine and the cancer stem cells in human breast cancer.

© 2010 Elsevier Inc. All rights reserved.

1. Introduction

Epidemiological studies have suggested that smoking is related to increased breast cancer risk [1]. Nicotine is considered to be most likely related to the risk in cigarette smoking [2]. Nicotine exerts its cellular functions through nicotinic acetylcholine receptors (nAChRs), which are heterodimers of nine different types of α subunits (α2–α10) and three kinds of β subunits (β2–β4). Recent studies have shown that nAChRs are present in a variety of cells, such as cancer cells, brain, and vascular smooth muscle cells [2–4]. However, little is known about the relationship between nicotine and the increased risk of breast cancer.

There is increasing evidence that many types of cancer, including breast cancer, are initiated from and maintained by a small population of cancer stem cells [5,6]. This minor population produces the cancer bulk through continuous self-renewal and differentiation, which contributes to the cancer cellular heterogeneity. Aldehyde dehydrogenase (ALDH), which is a detoxifying enzyme responsible for the oxidation of intracellular aldehydes, has been recently used as a functional marker for identification of cells with enhanced tumorigenic/metastatic potential [7–9]. In addition, ALDH-positive cells from breast tissue can be used as a predictor of clinical outcome in breast cancer patients [10].

The self-renewal behavior of cancer stem cells has been reported to be mediated by several signaling pathways, such as Notch, Hedgehog, and Wnt [11–13]. Notch might be important for breast cancer stem cells. Transgenic mice overexpressing isoforms of Notch, a signaling pathway active in stem cells, are more prone to develop mammary tumors [14]. Furthermore, the expression level of Notch-1 and Jagged-1 has been shown to correlate with poor prognosis [15]. Aberrant Notch-1 activation was reported in breast carcinomas of various subtypes [16].

In the present study, we investigated the effects of nicotine on the population of cancer stem cells in MCF-7 human breast cancer cells, using flow cytometry with the cancer stem cell marker aldehyde dehydrogenase (ALDH). We report here that nicotine increases stem cell population in MCF-7 cells. In addition, our data suggest that the effect of nicotine is mediated via the α7 subunits of nAChR and the PKC-Notch dependent pathway in MCF-7 cells. These findings might explain the development of breast cancer in cigarette smokers.

2. Materials and methods

2.1. Materials

Nicotine was from Wako Pure Chemicals (Osaka, Japan). Mecamylamine hydrochloride (MCA) and PHA543613 (*N*-[(3R)-1-Azabicyclo[2.2.2]oct-3-yl]furo[2,3-c]pyridine-5-carboxamide) were from Sigma–Aldrich (St. Louis, MO, USA). α-Bungarotoxin was from Tocris Bioscience (Bristol, UK). GF109203X (3-[1-[3-(dimethylamino)propyl]-1H-indol-3-yl]-4-(1H-indol-3-yl)-1H-pyrrole-2,5-

* Corresponding author. Address: Division of Pharmacology, National Institute of Health Sciences, 1-18-1, Kamiyoga, Setagaya 158-8501, Japan. Fax: +81 3 3700 9704.
E-mail address: kanda@nihs.go.jp (Y. Kanda).

0006-291X/$ - see front matter © 2010 Elsevier Inc. All rights reserved.
doi:10.1016/j.bbrc.2010.10.134

dione monohydrochloride) and DAPT (*N*-[*N*-(3,5-difluorophenacetyl)-L-alanyl]-*S*-phenylglycine *t*-butyl ester) were from Enzo Life Sciences (Farmingdale, NY, USA). All other reagents were of analytical grade and obtained from commercial sources.

2.2. Cell culture

MCF-7 cells were provided from the American Type Culture Collection and cultured in Dulbecco's modified Eagle's medium (DMEM, #D6046, Sigma–Aldrich) supplemented with 10% heat-inactivated fetal bovine serum (FBS, Biological Industries, Ashrat, Israel), 100 U/ml penicillin and 100 μg/ml streptomycin (Gibco BRL, Invitrogen Corp., Carlsbad, CA, USA).

2.3. Aldefluor assay

The Aldefluor kit (Stem Cell Technologies, Durham, NC, USA) was used to detect stem cell population with high ALDH enzyme activity. Briefly, the cells were plated at 3×10^5 cells/100 mm dish. After serum deprivation for 3 days, the cells were suspended in Aldefluor assay buffer containing the ALDH substrate BAAA (1 μM) and incubated for 30 min at 37 °C. As a negative control, cells were treated with diethylaminobenzaldehyde (15 μM), which is a specific ALDH inhibitor. FACS Aria II cell sorter (BD Biosciences, San Diego, CA, USA) was used to measure the ALDH-positive cell population.

2.4. Mammosphere-forming assay

Mammosphere-forming assay was performed as previously described with slight modification [17]. Briefly, MCF-7 cells were plated on ultra-low attachment 6-well plates (Corning, Acton, MA, USA) at a density of 10,000 cells/ml in serum-free DMEM supplemented with N_2 supplement (Gibco) and 20 ng/ml basic Fibroblast Growth Factor (R&D Systems, Minneapolis, MN, USA). The number of spheres was microscopically analyzed.

2.5. Real-time RT-PCR

Total RNA was isolated from MCF-7 cells using ISOGEN (Nippon Gene, Osaka, Japan), according to the manufacturer's instructions. Quantitative real-time reverse transcription (RT)-PCR with a QuantiTect SYBR Green RT-PCR Kit (QIAGEN, Valencia, CA, USA) was performed using the ABI PRISM 7900HT sequence detection system (Applied Biosystems, Foster City, CA, USA). The relative changes in the amount of transcripts in each sample were determined by normalizing with the GAPDH mRNA levels. The sequences of the primers used for real-time PCR analysis are as follows: Hes-1 (forward, 5′-AGCGGGCGCAGATGAC-3′; reverse, 5′-CGTTCATGCACTCG CTGAA-3′), GAPDH (forward, 5′-GTCTCCTCTGACTTCAACAGCG-3′; reverse, 5′-ACCACCCTGTTGCTGTAGCCAA-3′).

2.6. Conventional RT-PCR

RT was performed in a 20-μl reaction volume comprising 1 μg total RNA, 1× reaction buffer, 0.5 mM dNTP mixture, 2.5 μM oligo(dT) primer, 40 U RNase OUT, and 200 U Superscript III reverse transcriptase (Invitrogen). PCR was performed using a thermal cycler (Gene Amp PCR System 2400-R, Perkin–Elmer, Norwalk, CT, USA) in a 20-μl reaction volume comprising 0.2 μl RT product, 1× PCR buffer, 0.5 μM each of the sense and antisense primers, and 0.1 U long and accurate Taq (Sigma–Aldrich). The following primers were used: α7-nAchR (forward, 5′-CGGAGTCAACGGATT GGTCGTAT-3′; reverse, 5′-CAGCGTACATCGATGTAGCA-3′); GAPDH (forward, 5′-CGGAGTCAACGGATTGGTCGTAT-3′; reverse, 5′-AGCCT TCTCCATGGTGGTGAAGAC-3′). The cycling conditions were as follows: 1 min at 94 °C, 40 cycles of 30 s at 94 °C, 30 s at 54 °C, and 30 s at 72 °C, followed by 7 min at 72 °C.

2.7. PKC activity

PKC activity was measured using a Pep Tag Non-Radioactive PKC Assay kit (Promega, Madison, WI, USA), according to the manufacturer's instructions. Briefly, MCF-7 cells were starved for 4 h and then stimulated with nicotine for 30 min. After the cells were lysed in a PKC extraction buffer, the cell lysates were incubated with the specific peptide substrate and the reaction buffer for 30 min at 30 °C. The reaction was stopped by placing the tube in a 95 °C heating block for 5 min. The samples were then separated on a 1% agarose gel at 100 V for 15 min. The phosphorylated bands were extracted from the gel and the intensity of the bands was measured at 570 nm using a microplate reader (iMark; Bio-Rad, Hercules, CA, USA).

2.8. Statistical analysis

The values are expressed as the arithmetic mean ± SD of three independent experiments. The data were statistically analyzed using two-tailed Student's *t*-test. Results were considered statistically significant if $P < 0.05$.

3. Results

3.1. Nicotine increases ALDH-positive cell population in MCF-7 cells

To investigate whether nicotine affects the size of stem cell population, we performed the Aldefluor assay, which is used for the identification of cancer stem cells, in human MCF-7 breast cancer cells. As shown in Fig. 1A, stimulation with 1 μM nicotine increased the ratio of ALDH-positive cell population. Nicotine increased both ALDH-positive cells (from 3.52×10^2 to 9.43×10^2 cells; approximately 2.7-fold) and ALDH-negative cells (from 3.16×10^5 to 3.47×10^5 cells; approximately 1.1-fold), suggesting that the effect of nicotine is due to the proliferation of the ALDH-positive cells. As shown in Fig. 1B, the effect of nicotine was observed in a dose-dependent manner and maximal effects were achieved at a concentration of 1 μM. To confirm whether nicotine increases the stem cell population, we measured the mammosphere-forming ability, which is used for self-renewal capability [17]. We found that the nicotine-treated MCF-7 cells formed approximately 2.0-fold more mammospheres than untreated control cells (Fig. 1C), suggesting that nicotine induces the stem cell proliferation. To examine whether the effect of nicotine is mediated through its nAChR, we tested the effects of a nAChR antagonist on the ALDH-positive cell population. As shown in Fig. 1D, a nAChR antagonist MCA inhibited the nicotine-induced increase in ALDH-positive cell population. MCA alone did not affect the ALDH-positive cell population. Taken together, these data suggest that nicotine increases ALDH-positive cell population via its nAChR in MCF-7 cells.

3.2. Nicotine induces a Notch-Hes1 pathway in MCF-7 cells

To investigate whether the effects of nicotine is involved in a stem cell-dependent pathway, we examined the Notch pathway, which is a feature of cancer stem cells. We found that nicotine induced an expression of Notch target gene Hes1 in MCF-7 cells (Fig. 2A). We next tested the effect of DAPT, which inhibits cleavage of activated Notch receptors by γ-secretase, and thereby prevents Notch signaling. DAPT reduced the nicotine-induced Hes1 expression (Fig. 2A) and the nicotine-induced increase in ALDH-positive cell population (Fig. 2B). These data suggest that nicotine in-

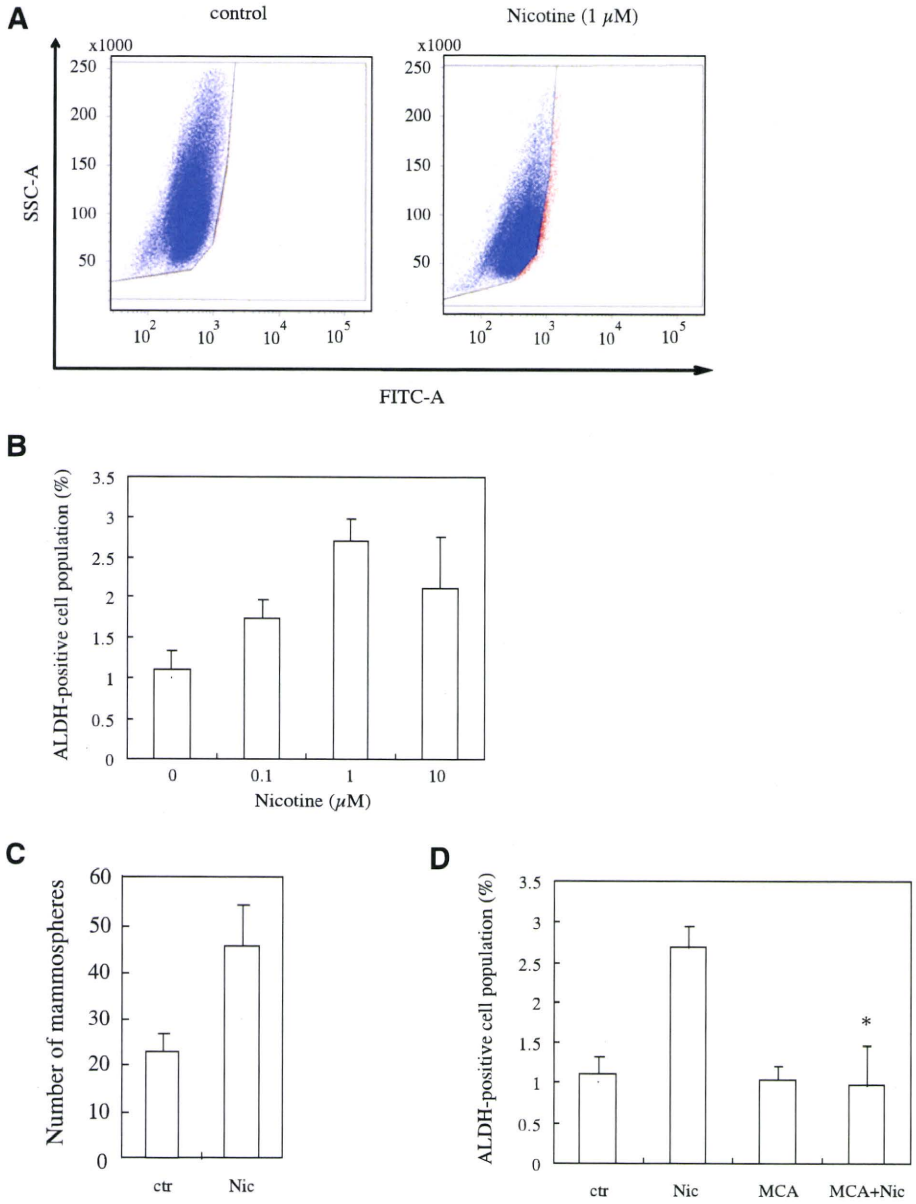

Fig. 1. Nicotine increases the stem cell population in MCF-7 cells. (A) MCF-7 cells were incubated with 1 μM nicotine for 72 h and the ALDH-positive cell population was measured by the Aldefluor assay kit and flow cytometry. (B) Effects of various concentrations of nicotine on ALDH-positive cell population. (C) After MCF-7 cells were stimulated with 1 μM nicotine, mammosphere-forming assay was performed in ultra-low attachment plates. (D) After MCF-7 cells were pretreated with the nicotine antagonist Mecamylamine (MCA, 10 μM), the cells were stimulated with 1 μM nicotine and then ALDH-positive cell population was measured. Values represent the mean ± SD from three independent experiments. $^*P < 0.05$ as compared with the respective control.

creases the ALDH-positive cell population via a Notch-Hes1 pathway in MCF-7 cells.

3.3. Effect of PKC on stem cell population in MCF-7 cells

Since protein kinase C (PKC) has been shown to be activated by nicotine and correlated with aggressiveness in breast tumor [18,19], we studied whether PKC is involved in the ALDH-positive cell population in MCF-7 cells. The potent PKC inhibitor GF109203X inhibited the nicotine-induced Hes1 expression (Fig. 3A) and nicotine-induced ALDH-positive cell population (Fig. 3B), suggesting that Notch act at a downstream of PKC. In addition, nicotine induced PKC activation via nAChR in MCF-7 cells. GF109203X inhibited the nicotine-induced PKC activation in MCF-7 cells (Fig. 3C). These data suggest that nicotine-induced PKC activation mediates the Notch pathway to drive the ALDH-positive cell population in MCF-7 cells.

3.4. Effect of α7 nAChR on stem cell population

We further investigated the subtype of nAChR. Since A549 human alveolar epithelial cells and other cancer cells are known to express α7-nAChR [4], we examined the involvement of α7-nAChR in stem cell population. As shown in Fig. 4A, α7-nAChR was detected in MCF-7 cells by RT-PCR. A549 cells were used as a positive control. As shown in Fig. 4B, the α7-selective nAChR agonist PHA543613 increased the ALDH-positive cell population in a dose-dependent manner. Furthermore, α-Bungarotoxin, an α7-

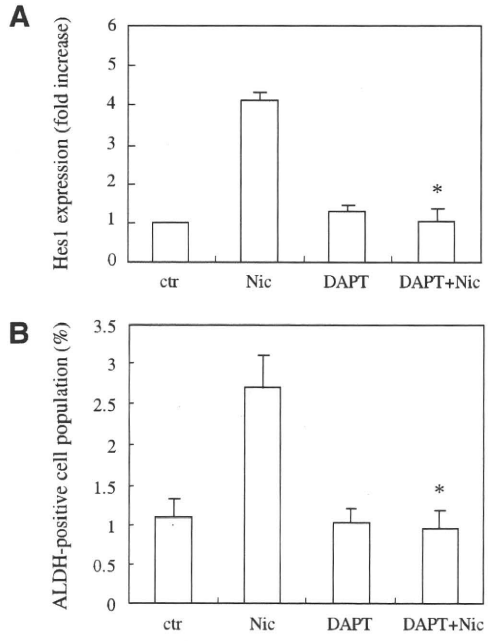

Fig. 2. Effect of a Notch-Hes pathway on the stem cell population in MCF-7 cells. (A) MCF-7 cells were pretreated with the α7-nAChR antagonist BTX (1 μM) or the Notch inhibitor DAPT (5 μM) and then stimulated with 1 μM nicotine. Hes1 expression was measured by real-time RT-PCR. (B) After MCF-7 cells were pretreated with DAPT, the cells were stimulated with 1 μM nicotine and then the ALDH-positive cell population was measured. Values represent the mean ± SD from three independent experiments. $^*P < 0.05$ as compared with the respective control.

selective nAChR antagonist, inhibited the nicotine-induced increase in ALDH-positive cell population in MCF-7 cells (Fig. 4C). α-Bungarotoxin also inhibited the nicotine-induced Hes1 expression and PKC activation (Fig. 4D and E). These data suggest that nicotine increases the ALDH-positive cell population via α7-nAChR in MCF-7 cells.

4. Discussion

In the present study, we demonstrated that nicotine increases the stem cell population in MCF-7 cells. We found the α7-nAChR as a mediator of the stem cell population. Furthermore, we showed that the Notch-Hes1 pathway act at the downstream of nAChR in the stem cell population.

There is increasing evidence regarding the existence of breast cancer stem cells and their central role in tumorigenesis. Clinical studies have suggested that smokers have enhanced metastasis of breast cancers to the lung [20,21]. These data raise the possibility that nicotine affect breast cancer stem cells. Our findings suggest that 1 μM nicotine increases ALDH-positive cell population via nAChR in MCF-7 cells. Since the plasma concentration of nicotine was reported to range between 10 nM and 10 μM in cigarette smokers [22], the concentrations of nicotine tested in our study are closely related to the blood concentrations of nicotine in cigarette smokers and might possibly induce growth or differentiation of breast cancer stem cells. Our observations support the idea that nicotine is related to the development of breast cancer in cigarette smokers.

We identified α7-nAChR as the major mediators of the stem cell population. Nicotine is known to activate many signaling cascade, such as Src, PI-3kinase, Akt signaling via nAChR [22]. Since the targeting of these pathways is not considered to be highly selective against cancer, α7-nAChR might be a good target for anti-cancer

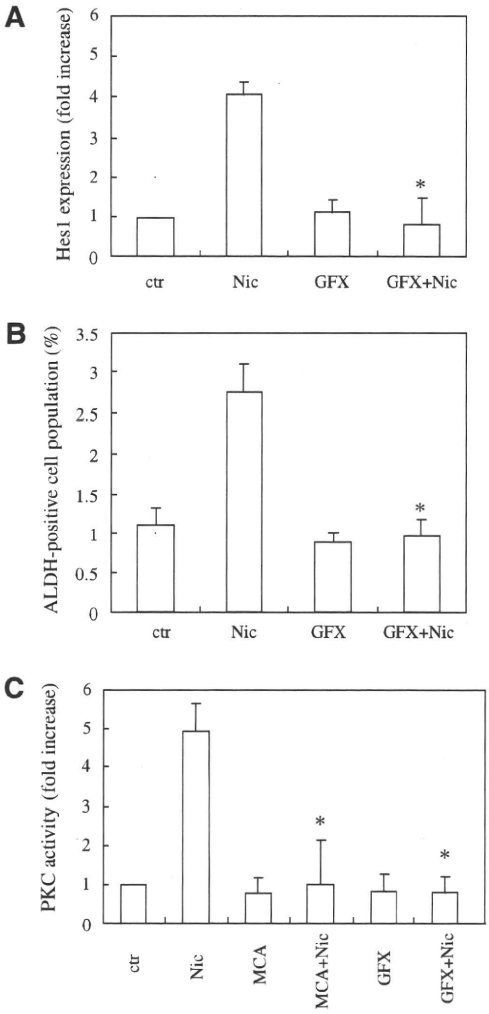

Fig. 3. Role of PKC on the stem cell population in MCF-7 cells. (A) After pretreatment with or without a PKC inhibitor GF109203X (GFX; 1 μM), MCF-7 cells were stimulated with 1 μM nicotine. Hes1 expression was measured by real-time RT-PCR. (B) After MCF-7 cells were pretreated with GFX, the cells were stimulated with 1 μM nicotine and then the ALDH-positive cell population was measured. (C) After MCF-7 cells were stimulated with 1 μM nicotine for 30 min, PKC activity was measured using a non-RI method. Values represent the mean ± SD from three independent experiments. $^*P < 0.05$ as compared with the respective control.

agents. We are currently conducting studies to examine the effect of α7-nAChR on in vivo tumorigenicity from breast cancer stem cells.

Our study demonstrated that nicotine increased the expression of the Notch target gene Hes1 and the stem cell population. Since Notch signaling has been shown to be required in mammosphere formation [12], our results using ALDH assay confirm a role for Notch signaling in breast cancer stem cells. However, the mechanism of how nicotine activates the Notch-dependent pathway is not well understood. ADAM protease has been implicated in the cleavage of Notch receptors [23]. Since PKC activity induces ADAM membrane translocation in glioblastoma [24], nicotine might activate ADAM by PKC and thereby induce Notch activation and the stem cell population in MCF-7 cells.

Cigarette smoking contains over 4000 different chemicals, many of which are toxic and/or carcinogenic in a variety of cells including breast epithelial cells [25,26]. Whereas we show nicotine

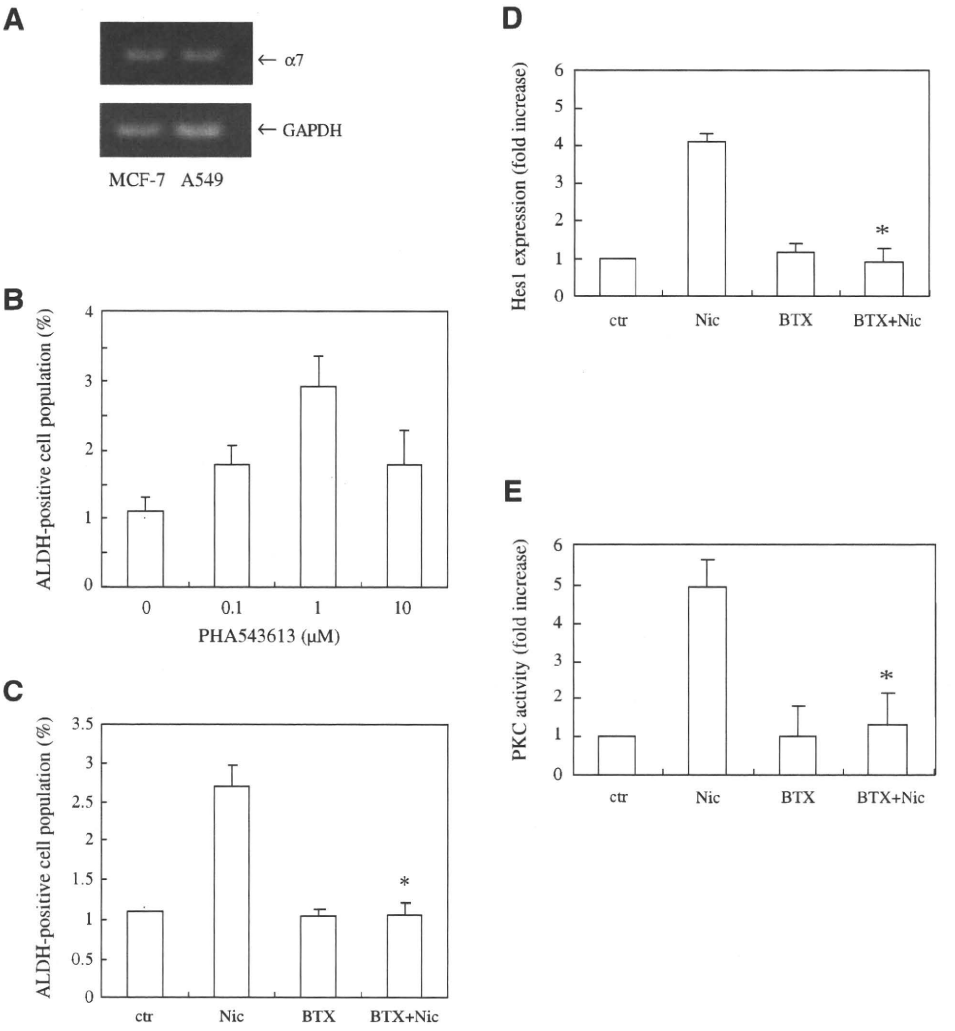

Fig. 4. Effect of α7-nAChR on the stem cell population in MCF-7 cells. (A) The α7-nAChR were detected by RT-PCR in MCF-7 cells. (B) MCF-7 cells were incubated with various concentrations of a α7-nAChR-selective agonist (PHA543613) and then the ALDH-positive cell population was measured. (C) After MCF-7 cells were pretreated with the α7-nAChR antagonist α-Bungarotoxin (BTX, 1 μM), the cells were stimulated with 1 μM nicotine and then the ALDH-positive cell population was measured.(D) MCF-7 cells were pretreated with the α7-nAChR antagonist BTX (1 μM) and then stimulated with 1 μM nicotine. Hes1 expression was measured by real-time RT-PCR. (E) MCF-7 cells were pretreated with the α7-nAChR antagonist BTX (1 μM) and then stimulated with 1 μM nicotine for 30 min. PKC activity was measured using a non-RI method. Values represent the mean ± SD from three independent experiments. *$P < 0.05$ as compared with the respective control.

increases the stem cell population, there are numerous other molecules in cigarette smoking that can affect cancer stem cells. NNK, which is a nicotine-derived nitrosamino ketone, has been found to transform human normal breast cells [27]. Thus, NNK also might contribute to the observed stem cell population. Future studies would be required to examine whether the other cigarette components are involved in breast cancer stem cells.

In conclusion, we show here that nicotine increases the stem cell population via α7-nAChR in MCF-7 cells. These findings reveal a novel role for nicotine as a stimulant of the cancer stem cell population in human breast cancer. These findings might explain the development of breast cancer in cigarette smokers. Development of agents that can disrupt the α7-nAChR signaling pathway may provide a new therapeutic way for the treatment of breast cancer.

Conflicts of interest statement

None declared.

Acknowledgments

We thank Dr. Waka Lin for critical reading of the manuscript. This work was supported in part by a grant from the Program for Promotion of Fundamental Studies in Health Sciences of the National Institute of Biomedical Innovation (NIBIO) (No. 09-02 to Y.K.), a Grant-in-Aid for Young Scientists (B) from the Ministry of Education, Culture, Sports, Science, and Technology, Japan (No. 2179025 to Y.K.), and a grant from the Smoking Research Foundation (Y.K.).

References

[1] S.S. Hecht, DNA adduct formation from tobacco-specific N-nitrosamines, Mutat. Res. 424 (1999) 127–142.
[2] B.M. Conti-Fine, D. Navaneetham, S. Lei, A.D. Maus, Neuronal nicotinic receptors in non-neuronal cells: new mediators of tobacco toxicity? Eur. J. Pharmacol. 393 (2000) 279–284.

[3] Y. Kanda, Y. Watanabe, Nicotine-induced vascular endothelial growth factor release via the EGFR-ERK pathway in rat vascular smooth muscle cells, Life Sci. 80 (2007) 1409–1414.
[4] R.D. Egleton, K.C. Brown, P. Dasgupta, Nicotinic acetylcholine receptors in cancer: multiple roles in proliferation and inhibition of apoptosis, Trends Pharmacol. Sci. 29 (2008) 151–158.
[5] S. Liu, G. Dontu, M.S. Wicha, Mammary stem cells, self-renewal pathways, and carcinogenesis, Breast Cancer Res. 7 (2005) 86–95.
[6] H. Korkaya, A. Paulson, E. Charafe-Jauffret, C. Ginestier, M. Brown, J. Dutcher, S.G. Clouthier, M.S. Wicha, Regulation of mammary stem/progenitor cells by PTEN/Akt/β-catenin signaling, PLoS Biol. 7 (2009) e1000121.
[7] E. Charafe-Jauffret, C. Ginestier, F. Iovino, J. Wicinski, N. Cervera, P. Finetti, M.H. Hur, M.E. Diebel, F. Monville, J. Dutcher, M. Brown, P. Viens, L. Xerri, F. Bertucci, G. Stassi, G. Dontu, D. Birnbaum, M.S. Wicha, Breast cancer cell lines contain functional cancer stem cells with metastatic capacity and a distinct molecular signature, Cancer Res. 69 (2009) 1302–1313.
[8] F. Jiang, Q. Qiu, A. Khanna, N.W. Todd, J. Deepak, L. Xing, H. Wang, Z. Liu, Y. Su, S.A. Stass, R.L. Katz, Aldehyde dehydrogenase 1 is a tumor stem cell-associated marker in lung cancer, Mol. Cancer Res. 7 (2009) 330–338.
[9] T. Tanei, K. Morimoto, K. Shimazu, S.J. Kim, Y. Tanji, T. Taguchi, Y. Tamaki, S. Noguchi, Association of breast cancer stem cells identified by aldehyde dehydrogenase 1 expression with resistance to sequential paclitaxel and epirubicin-based chemotherapy for breast cancers, Clin. Cancer Res. 15 (2009) 4234–4241.
[10] C. Ginestier, M.H. Hur, E. Charafe-Jauffret, F. Monville, J. Dutcher, M. Brown, J. Jacquemier, P. Viens, C.G. Kleer, S. Liu, A. Schott, D. Hayes, D. Birnbaum, M.S. Wicha, G. Dontu, ALDH1 is a marker of normal and malignant human mammary stem cells and a predictor of poor clinical outcome, Cell Stem Cell 1 (2007) 555–567.
[11] S. Liu, G. Dontu, I.D. Mantle, S. Patel, N.S. Ahn, K.W. Jackson, P. Suri, M.S. Wicha, Hedgehog signaling and Bmi-1 regulate self-renewal of normal and malignant human mammary stem cells, Cancer Res. 66 (2006) 6063–6071.
[12] G. Dontu, K.W. Jackson, E. McNicholas, M.J. Kawamura, W.M. Abdallah, M.S. Wicha, Role of Notch signaling in cell-fate determination of human mammary stem/progenitor cells, Breast Cancer Res. 6 (2004) R605–615.
[13] M.J. Smalley, T.C. Dale, Wnt signalling in mammalian development and cancer, Cancer Metastasis Rev. 18 (1999) 215–230.
[14] C. Hu, A. Dievart, M. Lupien, E. Calvo, G. Tremblay, P. Jolicoeur, Overexpression of activated murine Notch1 and Notch3 in transgenic mice blocks mammary gland development and induces mammary tumors, Am. J. Pathol. 168 (2006) 973–990.
[15] M. Reedijk, S. Odorcic, L. Chang, H. Zhang, N. Miller, D.R. McCready, G. Lockwood, S.E. Egan, High-level coexpression of JAG1 and NOTCH1 is observed in human breast cancer and is associated with poor overall survival, Cancer Res. 65 (2005) 8530–8537.
[16] S. Stylianou, R.B. Clarke, K. Brennan, Aberrant activation of notch signalling in human breast cancer, Cancer Res. 66 (2006) 1517–1525.
[17] G. Dontu, W.M. Abdallah, J.M. Foley, K.W. Jackson, M.F. Clarke, M.J. Kawamura, M.S. Wicha, In vitro propagation and transcriptional profiling of human mammary stem/progenitor cells, Gene Dev. 17 (2003) 253–1270.
[18] G.K. Lønne, L. Cornmark, I.O. Zahirovic, G. Landberg, K. Jirström, C. Larsson, PKC alpha expression is a marker for breast cancer aggressiveness, Mol. Cancer 9 (2010) 76.
[19] P. Dasgupta, W. Rizwani, S. Pillai, R. Kinkade, M. Kovacs, S. Rastogi, S. Banerjee, M. Carless, E. Kim, D. Coppola, E. Haura, S. Chellappan, Nicotine induces cell proliferation, invasion and epithelial-mesenchymal transition in a variety of human cancer cell lines, Int. J. Cancer 124 (2009) 36–45.
[20] S. Murin, J. Inciardi, Cigarette smoking and the risk of pulmonary metastasis from breast cancer, Chest 119 (2001) 1635–1640.
[21] S. Murin, K.E. Pinkerton, N.E. Hubbard, K. Erickson, The effect of cigarette smoke exposure on pulmonary metastatic disease in a murine model of metastatic breast cancer, Chest 125 (2004) 1467–1471.
[22] E.R. Gritz, V. Baer-Weiss, N.L. Benowitz, M.E. Van VunakisHjarvik, Plasma nicotine and cotine concentrations in habitual smokeless tobacco users, Clin. Pharmacol. Ther. 30 (1981) 201–209.
[23] E.C. Bozkulak, G. Weinmaster, Selective use of ADAM10 and ADAM17 in activation of Notch1 signaling, Mol. Cell Biol. 29 (2009) 5679–5695.
[24] Z.A. Kohutek, C.G. diPierro, G.T. Redpath, I.M. Hussaini, ADAM-10-mediated N-cadherin cleavage is protein kinase C-alpha dependent and promotes glioblastoma cell migration, J. Neurosci. 29 (2009) 4605–4615.
[25] D.M. DeMarini, Genotoxicity of tobacco smoke and tobacco smoke condensate: a review, Mutat. Res. 567 (2004) 447–474.
[26] C.N. Kundu, R. Balusu, A.S. Jaiswal, C.G. Gairola, S. Narayan, Cigarette smoke condensate-induced level of adenomatous polyposis coli blocks long-patch base excision repair in breast epithelial cells, Oncogene 26 (2007) 1428–1438.
[27] J. Mei, H. Hu, M. McEntee, H. Plummer 3rd, P. Song, H.C. Wang, Transformation of non-cancerous human breast epithelial cell line MCF10A by the tobacco-specific carcinogen NNK, Breast Cancer Res. Treat. 79 (2003) 95–105.

Forensic Science International 198 (2010) 62–69

Contents lists available at ScienceDirect

Forensic Science International

journal homepage: www.elsevier.com/locate/forsciint

Determination of a new designer drug, *N*-hydroxy-3,4-methylenedioxymethamphetamine and its metabolites in rats using ultra-performance liquid chromatography–tandem mass spectrometry

Ruri Kikura-Hanajiri *, Maiko Kawamura, Atsuko Miyajima, Momoko Sunouchi, Yukihiro Goda

National Institute of Health Sciences, 1-18-1, Kamiyoga, Setagaya, Tokyo 158-8501, Japan

ARTICLE INFO

Article history:
Received 21 August 2009
Received in revised form 29 January 2010
Accepted 9 February 2010
Available online 17 March 2010

Keywords:
N-OH MDMA
MDMA
MDA
Rats
Biological samples
UPLC–MS/MS

ABSTRACT

An *N*-hydroxy analogue of 3,4-methylendioxymethamphetamine (MDMA), *N*-hydroxy MDMA (*N*-OH MDMA), has recently been distributed as a new designer drug in some drug markets. Very little data is available to the metabolic and pharmacological properties of *N*-OH MDMA, although it has been reported that the *N*-demethyl analogue, *N*-hydroxy-3,4-methylenedioxyamphetamine (*N*-OH MDA), is mainly metabolized to MDA in rats. In this study, an analytical method for the determination of *N*-OH MDMA and its metabolites in biological samples was developed, and the metabolic properties of *N*-OH MDMA in rats were investigated.

After the *i.p.* administration of *N*-OH MDMA to pigmented hairy rats (5 mg/kg/day, 10 days), *N*-OH MDMA and its *N*-dehydroxy and *N*-demethyl metabolites (MDMA, *N*-OH MDA and MDA) in rat plasma, urine and hair samples were determined by ultra-performance LC (UPLC)–MS/MS. The hair sample was extracted by 1-h sonication and overnight soaking in 5 M hydrochloric acid–methanol (1:20). The plasma, urine, and hair extract samples were purified using a solid-phase extraction procedure. *N*-OH MDMA in the samples could be precisely analyzed by avoiding an alkaline environment. The parent compound very rapidly disappeared from the rat plasma (<15 min) and urine (<10 h), and most of the *N*-OH MDMA was excreted in the rat urine as MDMA and MDA in 72 h. In the rat hair samples collected 4 weeks after the first administration, *N*-OH MDMA (0.03 ng/mg) and *N*-OH MDA (0.13 ng/mg) were clearly detected as well as MDMA (149 ng/mg) and MDA (52 ng/mg). This analytical method will be useful for the analysis of *N*-OH MDMA and its metabolites in biological samples.

© 2010 Elsevier Ireland Ltd. All rights reserved.

1. Introduction

Various designer drugs of 3,4-methylenedioxymethamphetamine (MDMA) have appeared as street drugs in recent years. Besides *N*-alkyl derivatives of MDMA such as 3,4-methylenedioxyethylamphetamine (MDEA), the use of beta-keto compounds such as methylone, 1-(3,4-methylenedioxyphenyl-2-(pyrrolidin-1-yl)-1-pentanone (MDPV), 2-methylamino-1-(3,4-methylenedioxyphenyl)butan-1-one (bk-MBDB), and 2-ethylamino-1-(3,4-methylenedioxyphenyl)propan-1-one) (bk-MDEA) has become widely spread throughout the world [1–7]. Moreover, an *N*-hydroxyl analogue of MDMA, *N*-hydroxy MDMA (*N*-OH MDMA, FLEA), has also been distributed as a new designer drug in some drug markets [5,8].

The *N*-hydroxy group has been found to have unique analytical properties in similar compounds such as *N*-hydroxy-3,4-methylenedioxyamphetamine (*N*-OH MDA; *N*-demethyl analogue of *N*-OH MDMA). *N*-OH MDA is unstable at high temperatures (e.g. GC–MS analysis) and decomposes to MDA and the oxime of 3,4-methylenedioxyphenyl-2-propanone [9]. Moreover, *N*-OH MDA (p*K*a value = 6.22) is considerably less basic than MDA (p*K*a value = 10.04), and thus its capacity factors show greater variation with mobile phase pHs in the 2.5–6.0 range for HPLC analysis, while retention of the primary amine, MDA, and *N*-alkyl MDAs remains relatively constant over this range [10]. The aqueous solution stability of *N*-OH MDA has been found to decrease with increases in the aqueous solution pH, and the degradation half-life decreases to a value of 2.57 h at pH 10 [10]. In an alkaline environment, *N*-OH MDA is mainly transformed to its corresponding oxime. This pH-dependent mechanism is different from that in the pyrolysis of *N*-OH MDA, as observed in the GC–MS analysis. On the other hand, Ravis et al. [11] have reported that *N*-OH MDA is rapidly metabolized to MDA in rats and that no other major metabolites could be detected in a rat liver slice, plasma, or urine sample. As compared with *N*-OH MDA, very little data is available as to the analytical, metabolic, and pharmacological properties of

* Corresponding author. Tel.: +81 3 3700 8764; fax: +81 3 3707 6950.
E-mail address: kikura@nihs.go.jp (R. Kikura-Hanajiri).

0379-0738/$ – see front matter © 2010 Elsevier Ireland Ltd. All rights reserved.
doi:10.1016/j.forsciint.2010.02.013

N-OH MDMA, although it has been reported that direct GC–MS analysis of *N*-OH MDMA gives no indication of the parent compound and that only MDMA (*N*-dehydroxy compound) and MDA (*N*-dehydroxy and *N*-demethyl compound) are detected as the major components of the sample [8].

In this study, the stability of *N*-OH MDMA in sample solutions under various conditions (including wide pH ranges) was studied to establish suitable conditions for animal studies. Furthermore, a rapid and sensitive analytical method for the simultaneous determination of *N*-OH MDMA and its metabolites in rat plasma, urine, and hair samples was developed using ultra-performance liquid chromatography–tandem mass spectrometry (UPLC–MS/MS), and the metabolic properties of *N*-OH MDMA in rats were investigated.

2. Materials and methods

2.1. Chemicals and reagents

MDMA hydrochloride [12], MDA hydrochloride [12], *N*-OH MDA hydrochloride [13] and 2-methylamino-1-phenylpropane-2,3,3,3-d4 hydrochloride (methamphetamine(MA)-d4, used as an internal standard) [14] were prepared, as previously reported. *N*-OH MDMA oxalate was synthesized from 3,4-methylenedioxyphenetylacetone and *N*-methylhydroxylamine according to the procedure reported by Noggle et al. [9]. Its structure and purity were confirmed by the measurements of accurate mass, the infrared spectrum [8], GC–MS (acetylated derivatives) [8], LC–MS [8], and ^{1}H- and ^{13}C-nuclear magnetic resonance (NMR) [5]. The accurate mass of $[M+H]^+$ was *m/z* 210.11309 in the positive scan mode by AccuTOF JMS-T100 (JEOL, Tokyo, Japan). The error between the observed mass and the theoretical mass of $[M+H]^+$ ($C_{11}H_{16}NO_3$) was +0.07 mmu. The structures of these drugs are shown in Fig. 1. A solid-phase extraction column (Bond Elut Plexa, 30 mg/1 mL) was obtained from Varian (Harbor City, CA, USA), and the membrane filter (Ultrafree-MC, 0.45 μm) was from Millipore Corporation (Bedford, MA, USA). All other chemicals and solvents were of an analytical reagent grade or HPLC grade (Wako Chemicals, Osaka, Japan).

2.2. Instrumentation

The UPLC analysis was performed using a Waters Acquity Ultra-Performance™ liquid chromatography system (Waters, Milford, MA, USA). The separations were achieved using an Acquity HSS T3 column (100 mm × 2.1 mm i.d., 1.8 μm) from Waters (Milford, MA, USA). The column temperature was maintained at 40 °C, and the following gradient system was used with a mobile phase A (1% formic acid) and mobile phase B (1% formic acid/acetonitrile) delivered at 0.3 mL/min: 90% A/10% B (0 min)–70% A/30% B (8 min). The mobile phase was used as a wash solvent to avoid any carry-over from previous injections. The auto-sampler was maintained at 4 °C and the injection volume was 2 μL. The total run time for each sample analysis was 8.0 min. Quantitation was achieved by MS/MS detection in a positive ion mode using a Quattro Premier XE mass spectrometer (Waters, Milford, MA, USA) equipped with an electrospray ionization (ESI) interface. Quantification was performed using multiple reaction-monitoring (MRM) of the transitions of *m/z* 210.2 → 163.2 for *N*-OH MDMA (4.5 min), *m/z* 196.2 → 163.2 for *N*-OH MDA (3.9 min), *m/z* 194.3 → 163.2 for MDMA (3.3 min), *m/z* 180.2 → 163.2 for MDA (2.9 min), and *m/z* 154.2 → 92.1 for IS (3.1 min), with a scan time of 0.05 s per transition. The cone voltage and collision energy were set at 20 and 15 for *N*-OH MDMA, MDMA, and IS, and at 20 and 10 for *N*-OH MDA and MDA, respectively. The optimal MS parameters obtained were as follows: capillary 3.0 kV, source temperature 120 °C, and desolvation temperature 400 °C. Nitrogen was used as the desolvation and cone gas, with a flow rate of 800 and 50 L/h, respectively. Argon was used as the collision gas, with a flow rate of 0.25 mL/min. All data collected in the centroid mode were processed using MassLynx™ NT4.1 software with a QuanLynx™ program (Waters, Milford, MA, USA).

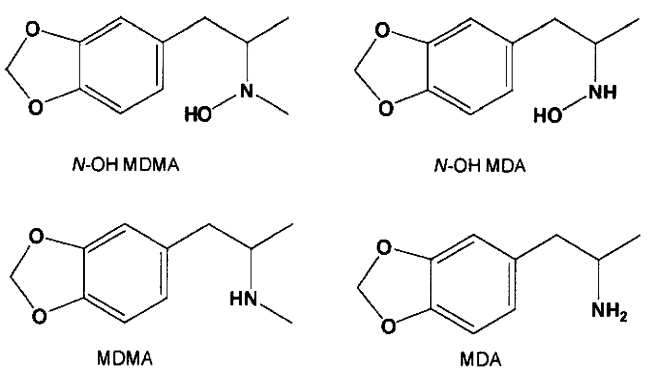

Fig. 1. Structures of *N*-OH MDMA and its metabolites.

2.3. Animal experiments

The animal experimental model was designed as shown in our previous reports [15,16]. All experiments were carried out with the approval of the Committee for Animal Care and Use of National Institute of Health Sciences, Japan. *N*-OH MDMA oxalate was administered to male dark agouti (DA) pigmented rats, which were 5 weeks old and around 90 g mean weight (Japan SLC, Shizuoka, Japan). The drugs were given once daily at 5 mg/kg by intraperitoneal injection for 10 successive days. Blood samples were collected 5, 15, 30, 60 120, and 360 min after the first administration from the orbital vein plexus. Plasma samples were prepared by centrifugation at 10,000 × *g* for 3 min and stored at −20 °C until analysis. The area under the plasma concentration time curve (AUC) was calculated by the conventional method [15]. Urine samples were collected 0–10, 10–24, 24–34, 34–48, and 48–72 h after the last administration and stored at −20 °C. To prevent the degradation of *N*-hydroxy compounds in the urine samples, 1 mL of 1 M phosphate buffer (pH 3) was added in advance to the collection vials and then cooled in an ice-bath (4 °C), and the pH of the collected urine was kept under acidic conditions. Each animal had been shaved on the back just before the first drug administration. The new growing hair samples were collected 28 days after the first administration.

2.4. Sample preparation

2.4.1. Stock solution

An individual standard solution of 1.0 mg/mL of each drug, *N*-OH MDMA, *N*-OH MDA, MDMA, and MDA, was prepared in methanol and stored at 4 °C. The IS solutions of 2 μg/mL of MA-d4 in methanol for the analysis of hair samples and those of 2 μg/mL of MA-d4 in distilled water for plasma and urine samples were also prepared.

2.4.2. Stability of *N*-OH MDMA

To investigate the stability of *N*-OH MDMA under various pH conditions, 0.5 mL of sample solutions containing 0.1 μg/mL of *N*-OH MDMA and MA-d4 (IS) were prepared with 0.1 M phosphate buffers at various pHs. The pHs of the buffer solutions, containing either mono- or di-basic potassium phosphate, were adjusted to 3.0, 4.0, 5.0, 6.0, 7.0, 8.0, 9.0, and 10.0 by adding 1 M phosphoric acid or 1 M potassium hydroxide, respectively. Fifty microliters of each sample solution was pipetted into the corresponding test tube, into which was previously added 0.45 mL of the mixed solution of methanol and acetonitrile (1:1) at 0, 1, 2, 4, 5, and 24 h after sample preparation, and analyzed using the UPLC–MS/MS system. The results were calculated using the peak-area ratios of the ions monitored for the target compounds versus IS, and indicated as a percentage of the remaining *N*-OH MDMA.

To establish suitable conditions for animal studies, *N*-OH MDMA and MA-d4 (IS) were dissolved in the rat drug-free urine (pH 8–9) at concentrations of 1 μg/mL. The stability of *N*-OH MDMA in the urine was studied under six different conditions described as follows: (1) kept at room temperature, (2) added 1 mL of 1 M phosphate buffer (pH 3.0) and kept at room temperature, (3) kept on ice, (4) added 1 mL of 1 M phosphate buffer (pH 3.0) and kept on ice, (5) the control urine was heated at 70 °C for 15 min before the addition of the drugs and was kept at room temperature, and (6) the urine was heated at 70 °C for 15 min and 1 mL of 1 M phosphate buffer (pH 3.0) was added before addition of the drugs. One hundred microliters of the sample under each condition was pipetted into the corresponding test tube, into which was previously added 1 mL of 0.1 M of phosphate buffer (pH 3.0) at 0, 1, 2, 4, 5, and 24 h after the sample preparation, and immediately the solution was treated with Bond Elut Plexa and analyzed as below. For the rat plasma samples, *N*-OH MDMA and MA-d4 (IS) were dissolved in the rat drug-free plasma (pH 7) at concentrations of 1 μg/mL. After being maintained at room temperature or on ice for 1, 2, and 4 h, 100 μL of each sample was pipetted and analyzed using the same method as with the urine samples.

2.4.3. Extraction of *N*-OH MDMA and its metabolites from plasma and urine samples

To a 50-μL plasma sample or a 100-μL urine sample were added 50 μL of the IS aqueous solution and 1 mL of 0.1 M phosphate buffer (pH 3.0), respectively. Before the quantitative analysis of MDMA and MDA, due to their high concentrations, the urine (0–10, 10–24, and 24–48 h) and plasma samples were diluted with the control specimens 100 times and 5 times as concentrations, respectively. After a Bond Elut Plexa was pre-activated with methanol and distilled water, the sample solution was applied to the Bond Elut Plexa. After the column was washed with 0.5 mL of distilled water, 0.5 mL of the solution of 2% formic acid/methanol was passed through the column to elute the target drugs. Following evaporation of the solvent under a nitrogen stream, the residue was dissolved in 0.5 mL of the mixed solution of methanol and acetonitrile (1:1). Two microliters of the solution was automatically injected into the UPLC–MS/MS.

2.4.4. Extraction of N-OH MDMA and its metabolites from hair samples

Hair samples were washed three times with distilled water under ultrasonication. After the sample was dried under a nitrogen stream at room temperature, approximately 10 mg of finely cut hair was precisely weighed and extracted with 1.5 mL of methanol/5 M hydrochloric acid mixed solution (20:1) containing 50 μL of each IS methanol solution for 1 h under ultrasonication. For the quantitative analysis of MDMA and MDA, 2-mg hair samples were used separately. Following overnight storage at room temperature, the hair was filtered off, the filtrate was evaporated with a nitrogen stream, and the residue was dissolved in 1 mL of 0.1 M phosphate buffer (pH 3.0). The solution was treated with Bond Elut Plexa and analyzed as above.

2.4.5. Linearity, precision, and recovery of the analytical method

The drug concentrations in the samples were calculated using the peak-area ratios of the ions monitored for the target compounds versus IS. The calibration curves for the determination were constructed by analyzing extracted drug-free control samples spiked with the standard solution, as described above. The calibration samples containing 0, 0.5, 1, 5, 10, 50, 100, and 500 ng/mL of the target drugs for the rat plasma and urine samples were prepared just before analysis. The samples containing 0, 0.01, 0.025, 0.05, 0.1, 0.25, 0.5, and 0.75 ng/mg of *N*-OH MDMA and *N*-OH MDA, and 0, 1, 2.5, 5, 10, 25, 50, and 75 ng/mg of MDMA and MDA for the hair samples were also prepared. For the urine analysis, 1 M phosphate buffer (pH 3.0) was added to the drug-free control urine samples before the addition of the standard solution of target drugs, to prevent the degradation of *N*-OH compounds. The limit of quantitation of each drug was chosen to be the concentration of the lowest calibration standard with an acceptable limit of variance.

The precision of the method was evaluated by five consecutive analyses of the plasma and urine samples that were spiked with the standard solutions containing 0.5, 50, and 500 ng/mL of the target drugs, respectively. For the hair analyses, the control samples, spiked with the standard solutions each containing 0.01, 0.05, and 0.5 ng/mg of *N*-OH MDMA and *N*-OH MDA and 1, 5, and 50 ng/mg of MDMA and MDA, were evaluated. The limit of detection (LOD) was defined as concentrations in a sample matrix resulting in peak areas with signal-to-noise (S/N) ratios of 3. The extraction recoveries of the four analytes, using the solid-phase extraction column, were determined using 0.1 M phosphate buffer (pH 3.0) spiked with the analytes at a concentration of 100 ng/mL, respectively. To determine the recoveries, the responses of the analytes spiked in the solutions before and after extraction were compared.

3. Results and discussion

3.1. Stability of N-OH MDMA

N-OH MDA, an *N*-demethyl analogue of *N*-OH MDMA, was unstable at high temperatures or in alkaline environments. It mainly decomposed to the oxime and/or its *N*-dehydroxy compound [9,10]. To evaluate the stability of *N*-OH MDMA oxalate in the stock solution, the methanol or aqueous solution of *N*-OH MDMA at a concentration of 1 mg/mL was kept at 4 °C for 2 weeks and the ratio of the remaining drug was measured. In both solutions, more than 90% of *N*-OH MDMA remained and thus they can be used as stock solutions for at least 2 weeks. In the same way, the stability of *N*-OH MDMA in the solution for the UPLC–MS/MS measurement was also studied. The ratios of the remaining drug of the solutions of 0.1% formic acid, acetonitrile, methanol, methanol/acetonitrile (1:1), 0.1% formic acid/10% acetonitrile (the initial composition of the mobile phase for the UPLC–MS/MS analysis) and 2% formic acid/methanol (the solution for eluting the drugs from the solid-phase extraction column) at a concentration of 0.1 μg/mL were analyzed over 24 h. As a result, the mixed solution of methanol/acetonitrile (1:1) was found to be the most suitable for the measurement of the UPLC–MS/MS system in this study.

To investigate the stability of *N*-OH MDMA under various pH conditions, the ratios of the remaining drugs in the buffer solutions under various pHs were analyzed over 24 h. *N*-OH MDMA was relatively stable in acidic conditions below pH 5, although it rapidly decomposed under basic conditions. Almost no parent compound was detected in the buffer solutions above pH 8 (Fig. 2). Beckett and Al-Sarraj [17] have reported that *N*-hydroxyamphetamine is readily decomposed into both the corresponding *syn*- and *anti*-oximes in alkaline solutions. The rate of the decomposition of *N*-hydroxyamphetamine is increased by dissolved oxygen in the solution, and a free radical mechanism has been proposed [17]. In contrast, Valaer et al. [10] have reported that *N*-OH MDA is chemically decomposed to its oxime and that this mechanism is pH-dependent. In our additional study, we detected the oxime- and nitroso-compounds of MDA as the decomposed products of *N*-OH MDMA in alkaline environments by NMR analyses [18]. Under these conditions, as compared with *N*-OH MDA, some other mechanism would be responsible for the chemical transformation of *N*-OH MDMA to its corresponding *N*-demethyl oxime- and nitroso-compounds.

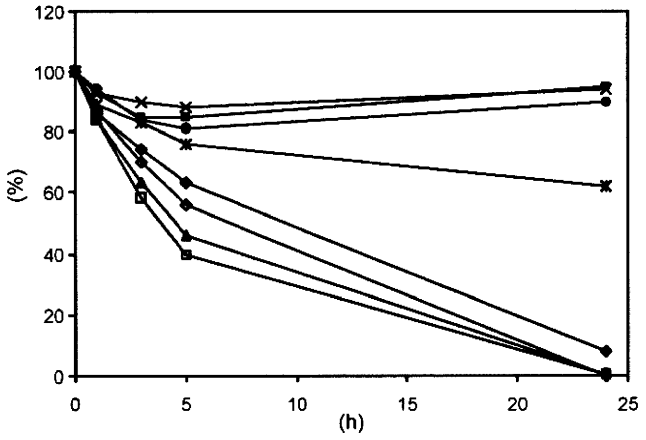

Fig. 2. Stabilities of *N*-OH MDMA oxalate in phosphate buffers at different pHs. ■, pH 3.0; ×, pH 4.0; ●, pH 5.0; *, pH 6.0; ◆, pH 7.0; ▲, pH 8.0; □, pH 9.0; ◇, pH 10.0.

Because of the instability of *N*-OH MDMA in an alkaline environment, it appears likely that this drug would decompose in rat urine samples (pH 8–9). To set suitable conditions for animal studies, the ratios of the remaining drug in the rat control urine (pH 8–9) with added *N*-OH MDMA were analyzed under six different conditions over 24 h (Fig. 3). The ratios of the remaining *N*-OH MDMA of the urine samples kept on ice were approximately 80% after 4 h and 50% after 24 h, while no *N*-OH MDMA was detected in the urine kept at room temperature after 24 h. When the urine samples were heated before adding the drugs to remove the influences of bacteria and endogenous enzymes, the ratios of the remaining drug were almost the same as those of the non-treated urine samples and no *N*-OH MDMA was detected after 24 h at room temperature. Furthermore, when the pH of the urine samples was adjusted to pH 4–5 before adding the drugs, the ratios of the

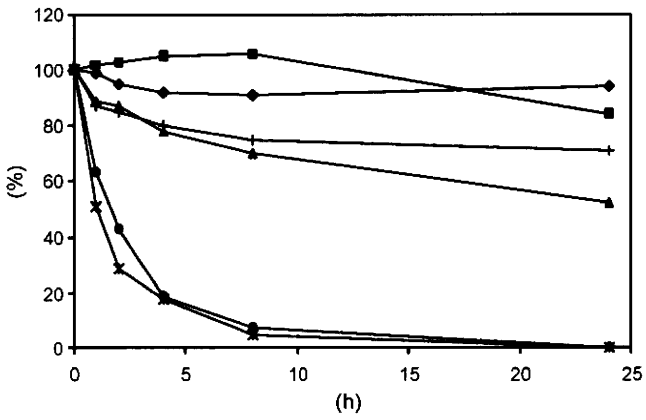

Fig. 3. Stabilities of *N*-OH MDMA oxalate in urine samples kept under different conditions. ●, kept at room temperature; ■, added 1 mL of 1 M phosphate buffer (pH 3.0) and kept at room temperature; ▲, kept on ice; ◆, added 1 mL of 1 M phosphate buffer (pH 3.0) and kept on ice; *, the control urine was heated at 70 °C for 15 min before addition of the drugs and was kept at room temperature, +, the urine was heated at 70 °C for 15 min and 1 mL of 1 M phosphate buffer (pH 3.0) was added before addition of the drugs.

Table 1
Linear ranges, calibration curves, and RSDs of analyses of *N*-OH MDMA and its metabolites in rat plasma, urine, and hair samples.

Compounds	Linear ranges	Calibration curves[a]	Conc. added	Conc. measured	RSDs (%)[b]
Plasma (ng/mL)					
N-OH MDMA	0.5–500		0.5	0.7	17
		$y = 0.5797x + 0.1111$	50.0	69.8	2.4
		$r^2 = 0.9988$	500.0	534.5	4.3
N-OH MDA	0.5–500		0.5	0.7	26
		$y = 0.4413x + 0.0647$	50.0	64.7	3.7
		$r^2 = 0.9983$	500.0	493.3	4.6
MDMA	0.5–500		0.5	0.3	7.1
		$y = 1.2243x + 0.2837$	50.0	58.5	2.3
		$r^2 = 0.9984$	500.0	513.2	2.3
MDA	0.5–500		0.5	0.4	17
		$y = 1.2047x + 0.2660$	50.0	61.8	1.8
		$r^2 = 0.9994$	500.0	530.9	1.8
Urine (ng/mL)					
N-OH MDMA	0.5–500		0.5	0.3	5.5
		$y = 0.8636x + 0.2218$	50.0	44.2	2.2
		$r^2 = 0.9981$	500.0	540.0	2.2
N-OH MDA	0.5–500		0.5	0.3	6.8
		$y = 0.3836x - 0.0111$	50.0	46.2	2.7
		$r^2 = 0.9983$	500.0	449.5	1.1
MDMA	0.5–500		0.5	0.3	6.9
		$y = 0.4741x + 0.2510$	50.0	53.0	2.5
		$r^2 = 0.9920$	500.0	522.7	16
MDA	0.5–500		0.5	0.3	27
		$y = 0.5269x + 0.2294$	50.0	45.2	4.9
		$r^2 = 0.9812$	500.0	465.3	2.1
Hair (ng/mg)					
N-OH MDMA	0.01–0.75		0.01	0.01	4.6
		$y = 4.8339 - 0.0019$	0.05	0.03	7.1
		$r^2 = 0.9900$	0.50	0.42	2.3
N-OH MDA	0.01–0.75		0.01	0.01	4.3
		$y = 2.3578 - 0.0056$	0.05	0.04	5.7
		$r^2 = 0.9892$	0.50	0.56	2.6
MDMA	1–50		1.0	1.2	2.5
		$y = 3.2766 + 0.8837$	5.0	5.2	2.4
		$r^2 = 0.9953$	50.0	53.1	1.5
MDA	1–50		1.0	1.1	2.5
		$y = 2.4426 + 0.2389$	5.0	5.5	1.9
		$r^2 = 0.9980$	50.0	55.3	1.2

[a] Weighting: $1/x$.
[b] RSD: relative standard deviation ($n = 5$).

Table 2
Time courses of drug concentrations in rat urine after the last administration of *N*-OH MDMA (5 mg/kg, *i.p.*).

Rat	Compounds	Concentrations in urine (μg/mL)				
		0–10 h	10–24 h	24–34 h	34–48 h	48–72 h
Rat 1	*N*-OH MDMA	0.05	TR	TR	TR	TR
	N-OH MDA	0.34	0.04	TR	TR	TR
	MDMA	75.3	12.4	1.97	0.68	0.17
	MDA	53.6	13.0	2.09	0.53	0.18
	Volume (mL)	2.5	5.3	2.8	3.6	6.2
Rat 2	*N*-OH MDMA	TR	TR	ND	ND	ND
	N-OH MDA	0.16	0.01	TR	TR	TR
	MDMA	63.4	7.35	1.79	0.73	0.36
	MDA	42.8	7.69	1.64	0.72	0.39
	Volume (mL)	2.7	4.3	3.0	3.6	6
Rat 3	*N*-OH MDMA	TR	TR	TR	ND	ND
	N-OH MDA	0.16	0.03	TR	TR	TR
	MDMA	69.9	12.5	3.43	0.64	0.66
	MDA	31.3	13.4	2.51	0.51	0.51
	Volume (mL)	3.5	3.8	3.0	2.8	3.7

TR: trace level, <10 ng/mL. ND: not detected.

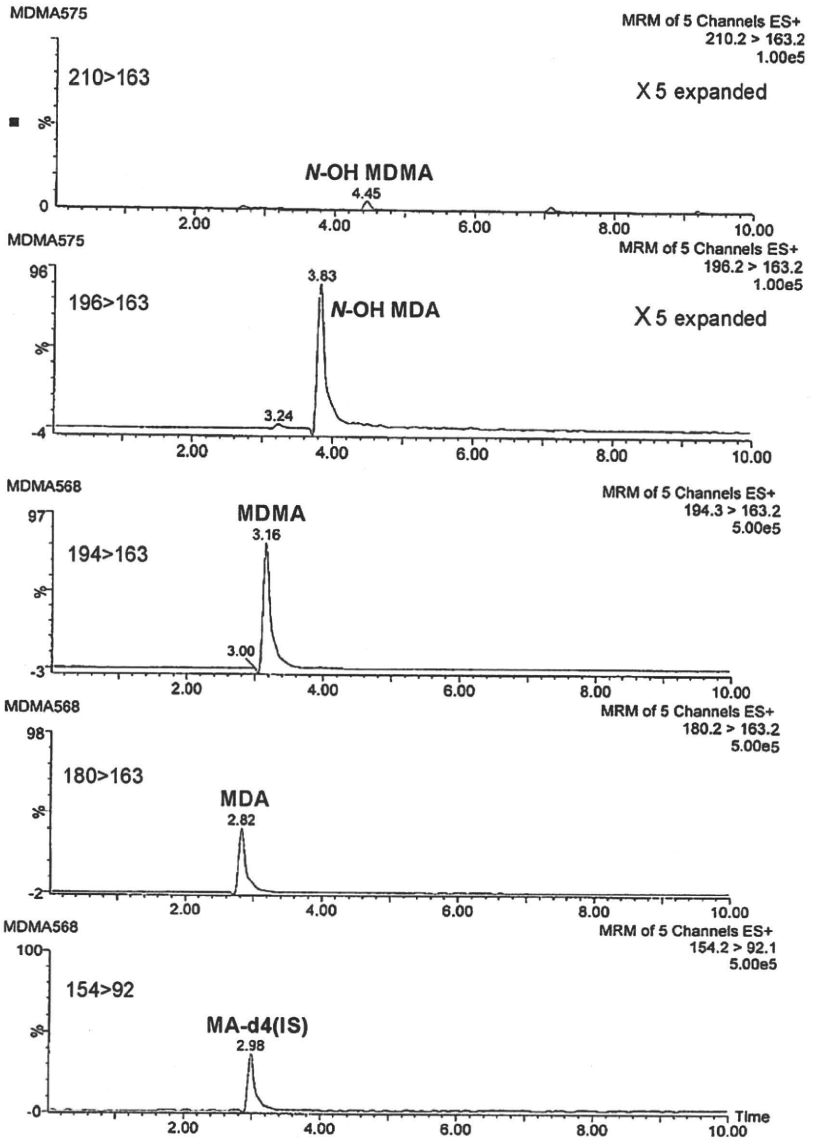

Fig. 4. UPLC–MS/MS MRM chromatograms of the extract from the rat urine 0–10 h after the last administration of *N*-OH MDMA (5 mg/kg, *i.p.*, rat 1).

remaining drugs after 24 h were approximately 95% on ice and 85% at room temperature (Fig. 3). On the basis of these results, adequate volumes of the phosphate buffer (pH 3.0) were added in advance to the collection vials in an ice-bath (4 °C), and the collected urine was kept under the acidic conditions in this study. On the other hand, no serious decomposition of *N*-OH MDMA in the plasma control samples kept on ice or at room temperature was observed for at least 2 h.

3.2. Pre-treatment steps

N-OH MDMA was unstable under the basic conditions, as described above. Moreover, it has been reported that *N*-OH MDA is considerably less basic than MDA and that its capacity factors show greater variation with mobile phase pH values for HPLC analysis using a C18 column [10]. Therefore, for the simultaneous extraction of target drugs from biological samples, a polymer-based solid-phase extraction column (Bond Elut Plexa™) was used without any basic solvents. According to the method described in Section 2, the recoveries of *N*-OH MDMA and its metabolites, *N*-OH MDA, MDMA, and MDA, from the samples added with their standard solutions (100 ng/mL), were 93.0, 85.5, 101.5 and 94.8%, respectively.

3.3. Linearity and precision of the analytical method for the rat urine, plasma, and hair samples

Under the chromatographic conditions used, there was no interference with any of the drugs or the internal standard by any extractable endogenous materials in the control rat plasma, urine, and hair extracts. The calibration curves were linear over the concentration range 0.5–500 ng/mL for rat plasma and urine, and 0.01–0.75 ng/mg (*N*-OH MDMA and *N*-OH MDA) and 1–50 ng/mg (MDMA and MDA) for rat hair with good correlation coefficients of $r^2 \geq 0.981$, respectively. The LODs of each drug were 0.1 ng/mL for the urine and plasma samples and 5 pg/mg for the hair samples, respectively. The precision data from the analytical procedure ($n = 5$) for the rat urine, plasma and hair samples, spiked with standard solution of *N*-OH MDMA, *N*-OH MDA, MDMA, and MDA, are presented in Table 1.

3.4. Time course of excretion of N-OH MDMA and its metabolites into rat urine

After intraperitoneal administration of *N*-OH MDMA oxalate to 3 rats at 5 mg/kg, the concentrations of *N*-OH MDMA and its metabolites in the rat urine were monitored using UPLC–MS/MS.

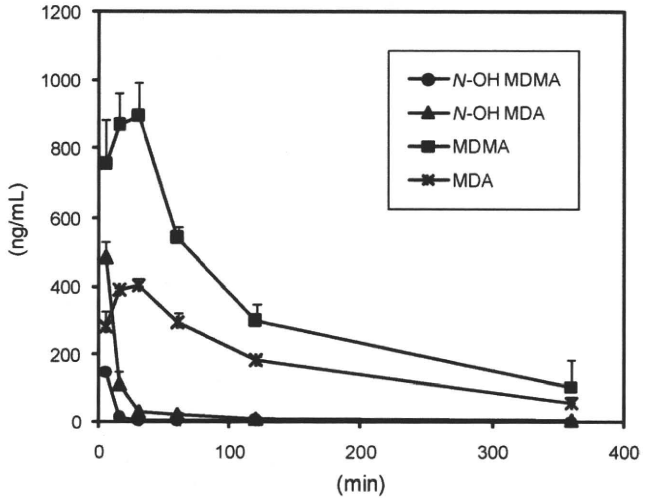

Fig. 5. Time courses of rat plasma drug concentrations after the first administration of *N*-OH MDMA (5 mg/kg, *i.p.*, $n = 3$). The error bar indicates each standard deviation.

The time courses of excretion of *N*-OH MDMA, *N*-OH MDA, MDMA, and MDA in the urine over 72 h are shown in Table 2. Fig. 4 shows LC–MS/MS MRM chromatograms of the extract from the rat urine 0–10 h after the last administration of *N*-OH MDMA (rat 1). The major metabolite excreted in the rat urine was MDMA (the *N*-dehydroxy metabolite), and 63–76 μg/mL of MDMA was detected from 0 to 10 h after administration. MDA (the *N*-dehydroxy and *N*-demethyl metabolite) was also detected at high concentrations of 31–54 μg/mL in the 0–10 h urine. In contrast, *N*-OH MDMA and *N*-OH MDA (the *N*-demethyl metabolite) were slightly detected only in 0–10 h urine and 0–24 h urine, and accounted for approximately 0.01 and 0.16% of the dose, respectively. More than 90% of the dose was excreted as MDMA and MDA in the rat urine in 72 h (Table 3), although other minor metabolites were not examined in this study. *N*-OH MDA has also been reported to be rapidly metabolized to MDA, and no other major metabolites have been detected in rats [11]. The rapid *N*-dehydroxylation of *N*-OH MDMA/*N*-OH MDA would make it difficult to discriminate *N*-OH MDMA/*N*-OH MDA use from MDMA/MDA use by urine analysis.

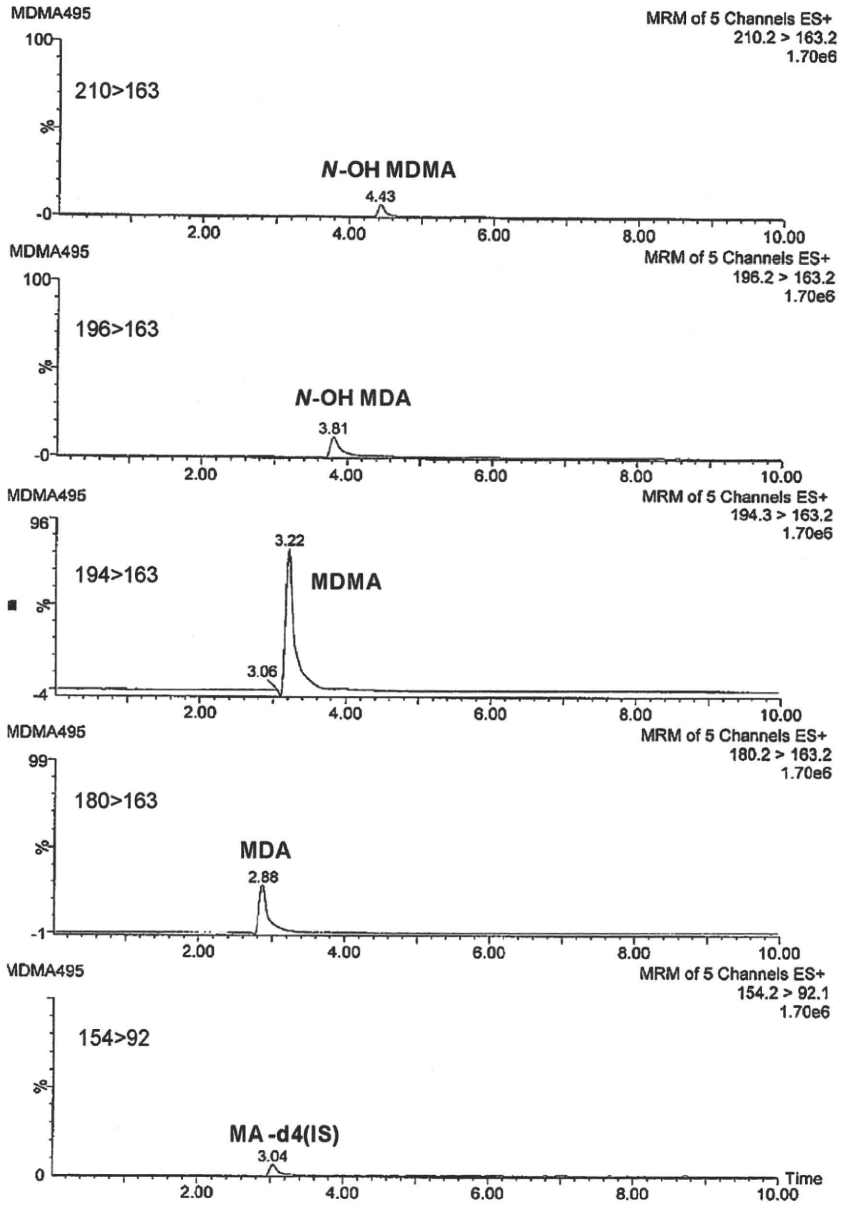

Fig. 6. UPLC–MS/MS MRM chromatograms of the extract from the rat plasma 5 min after the first administration of *N*-OH MDMA (5 mg/kg, *i.p.*, rat 1).

Table 3
The amounts of *N*-OH MDMA and its metabolites in urine, plasma, and hair.

Rat	Compounds	Total excretion into urine (μg, 0–72 h)	Plasma AUC (μg min/mL)	Concentrations in hair (ng/mg)
Rat 1	*N*-OH MDMA	0.1	1.1	0.03 ± 0.00
	N-OH MDA	1.1	7.2	0.07 ± 0.00
	MDMA	263.0	149.6	163.3 ± 1 7.3
	MDA	211.8	74.0	48.7 ± 0.7
Rat 2	*N*-OH MDMA	0.0	1.4	0.02 ± 0.00
	N-OH MDA	0.5	7.5	0.08 ± 0.00
	MDMA	212.9	130.9	117.6 ± 17.6
	MDA	158.8	77.6	41.4 ± 1.7
Rat 3	*N*-OH MDMA	0.0	1.4	0.03 ± 0.006
	N-OH MDA	0.7	10.2	0.23 ± 0.02
	MDMA	306.7	143.2	164.5 ± 11.1
	MDA	171.5	89.0	66.3 ± 1.4

3.5. Concentrations of *N*-OH MDMA and its metabolites in rat plasma

Fig. 5 shows the time courses of the rat plasma concentrations of *N*-OH MDMA and its metabolites over 360 min after the first administration of *N*-OH MDMA oxalate at 5 mg/kg. LC–MS/MS MRM chromatograms of the extract from the rat plasma 5 min after the administration of *N*-OH MDMA (Rat 1) are shown in Fig. 6. The concentrations of *N*-OH MDMA and *N*-OH MDA were

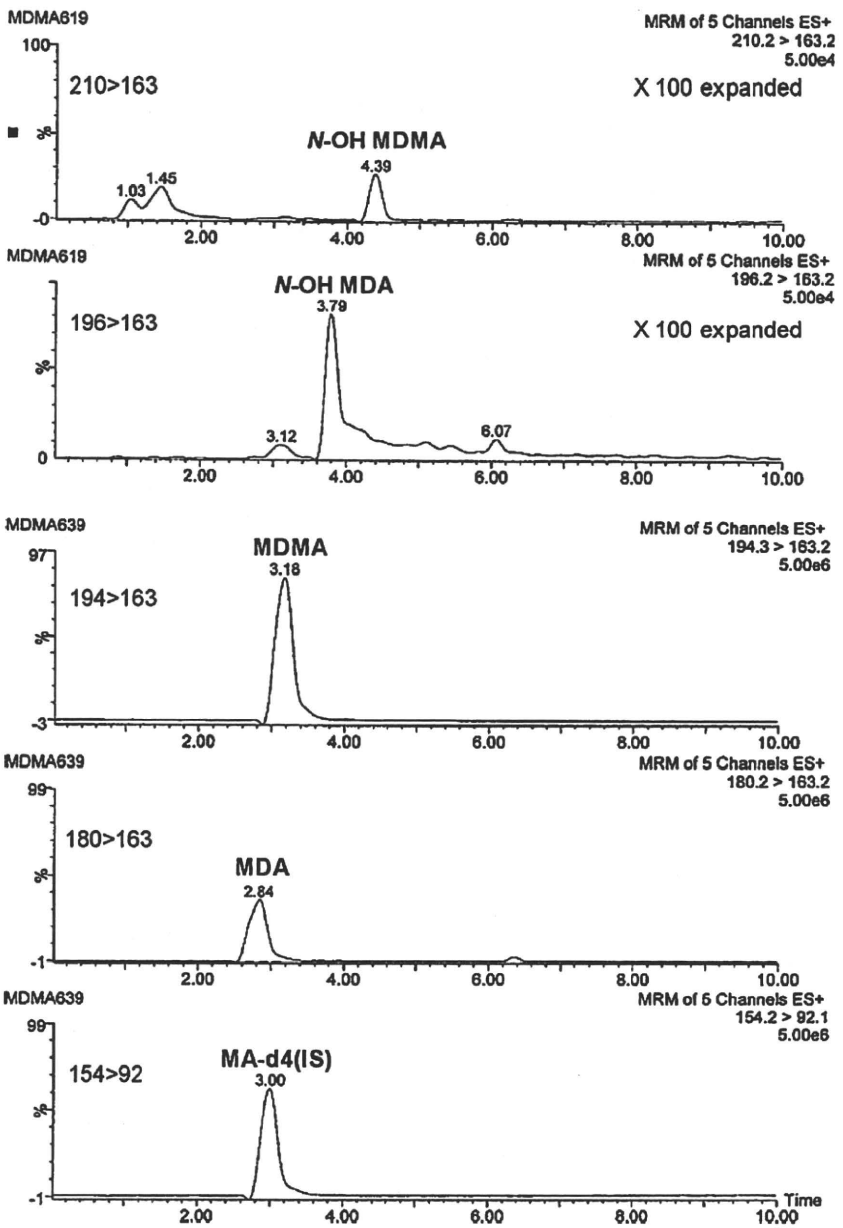

Fig. 7. UPLC–MS/MS MRM chromatograms of the extract from the rat hair collected 4 weeks after the first administration of *N*-OH MDMA (5 mg/kg × 10 days, *i.p.*, rat 1).

extremely low and their average peak concentrations ($n = 3$) were 130 ng/mg at 5 min and 490 ng/mL at 5 min, respectively. It was difficult to detect *N*-OH MDMA in the plasma at 120 min after administration. The concentrations of the major metabolites, MDMA and MDA in the plasma showed peaks (970 and 410 ng/mL) within 30 min. The AUC values of *N*-OH MDMA, *N*-OH MDA, MDMA, and MDA in the rat plasma were 1.1–1.4, 7.2–10.2, 130.9–149.6, and 74.0–89.0 μg min/mL, respectively, as shown in Table 3. The AUC values of MDMA and MDA were approximately 110 and 65 times larger than those of *N*-OH MDMA, respectively.

3.6. Drug concentrations in rat hair

Various procedures for the extraction of drugs from hair samples have been reported, including digestion with alkali, acid extraction, and enzymatic treatment [19,20]. Because *N*-OH MDMA is unstable under alkaline conditions, the procedures using alkali digestion (above pH 10) and enzymatic treatment (above pH 7) may not be acceptable for the extraction of *N*-OH MDMA. We have reported that the mixed solution of methanol and 5 M hydrochloric acid (20:1) is suitable for the extraction of phenethylamine-type compounds from hair samples [20,16]. Therefore, in this study, the acidic organic solvent was used for the extraction of *N*-OH MDMA and its metabolites from the rat hair. To investigate the stability of these drugs during the extraction procedure described in Section 2, the rat control hair samples, with added *N*-OH MDMA and its metabolites (10 ng/mg each), were analyzed. As a result of the analysis, almost no degradation of the *N*-OH compounds was observed.

Fig. 7 shows UPLC–MS/MS MRM chromatograms of the extract from the rat hair collected 4 weeks after the first administration of *N*-OH MDMA (5 mg/kg × 10 days, *i.p.*, rat 1). In the rat hair samples, although MDMA (149 ng/mg) and MDA (52 ng/mg) were mainly detected in large quantities, *N*-OH MDMA (0.03 ng/mg) and *N*-OH MDA (0.13 ng/mg) were also clearly detected. The detection of *N*-OH compounds from the hair samples might provide useful information for distinguishing *N*-OH MDMA use from MDMA use over a long period. However, it has been reported that *N*-OH MDMA and *N*-OH MDA are also detectable as *N*-hydroxylated metabolites in the urine of horses, orally administered with MDMA [21]. It may therefore be difficult to conclude whether *N*-OH MDMA detected in biological samples is the parent compound or the *N*-hydroxylated metabolite of MDMA. In further studies, the ratios of the parent compound to the metabolites in the samples obtained from *N*-OH MDMA users and MDMA users should be examined to deduce the source of the compound detected.

4. Conclusions

In this study, we have established a detailed procedure for the analysis of *N*-OH MDMA, *N*-OH MDA, MDMA, and MDA in rat urine, plasma, and hair samples using UPLC–MS/MS. Moreover, the established method was applied to investigate the metabolic properties of *N*-OH MDMA in rats. *N*-OH MDMA in biological samples could be precisely analyzed by avoiding alkaline environments. *N*-OH MDMA very rapidly disappeared from rat plasma and urine, and most of the *N*-OH MDMA was excreted in rat urine as MDMA and MDA in 72 h. The rapid *N*-dehydroxylation of *N*-OH MDMA would make it difficult to discriminate *N*-OH MDMA use from MDMA use by urine analysis. In the rat hair samples collected 4 weeks after the first administration, *N*-OH MDMA and *N*-OH MDA were clearly detected as well as MDMA and MDA, which were found to be the major metabolites in hair. The proposed analytical method will be useful for the analysis of *N*-OH MDMA and its metabolites in biological samples.

Acknowledgement

Part of this work was supported by a Health and Labor Sciences Research Grant from the Ministry of Health, Labor and Welfare in Japan.

References

[1] M.G. Bossong, J.P. Van Dijk, R.J. Niesink, Methylone and mCPP, two new drugs of abuse? Addict. Biol. 10 (4) (2005) 321–323.
[2] E. Shimizu, H. Watanabe, T. Kojima, H. Hagiwara, M. Fujisaki, R. Miyatake, K. Hashimoto, M. Iyo, Combined intoxication with methylone and 5-MeO-MIPT, Prog. Neuropsychopharmacol. Biol. Psychiatry 31 (1) (2007) 288–291.
[3] H.T. Kamata, N. Shima, K. Zaitsu, T. Kamata, A. Miki, M. Nishikawa, M. Katagi, H. Tsuchihashi, Metabolism of the recently encountered designer drug, methylone, in humans and rats, Xenobiotica 36 (8) (2006) 709–723.
[4] R. Kikura-Hanajiri, M. Kawamura, K. Saisho, Y. Kodama, Y. Goda, The disposition into hair of new designer drugs; methylone, MBDB and methcathinone, J. Chromatogr. B 855 (2) (2007) 121–126.
[5] N. Uchiyama, R. Kikura-Hanajiri, N. Kawahara, Y. Goda, Analysis of designer drugs detected in the products purchased in fiscal year 2006, Yakugaku Zasshi 128 (10) (2008) 1499–1505.
[6] K. Zaitsu, M. Katagi, H.T. Kamata, T. Kamata, N. Shima, A. Miki, H. Tsuchihashi, Y. Mori, Determination of the metabolites of the new designer drugs bk-MBDB and bk-MDEA, Forensic Sci. Int. 188 (1–3) (2009) 131–139.
[7] F. Westphal, T. Junge, P. Rösner, F. Sönnichsen, F. Schuster, Mass and NMR spectroscopic characterization of 3,4-methylenedioxypyrovalerone: a designer drug with alpha-pyrrolidinophenone structure, Forensic Sci. Int. 190 (1–3) (2009) 1–8.
[8] F.T. Noggle, C.R. Clark, J. DeRuiter, P. Cain, Analytical properties of *N*-hydroxy-3,4-methylenedioxymethamphetamine (FLEA), a potential new street drug, Microgram XXIX (1) (1996) 10–21.
[9] F.T. Noggle Jr., C.R. Clark, A.K. Valaer, J. DeRuiter, Liquid chromatographic and mass spectral analysis of *N*-substituted analogues of 3,4-methylenedioxyamphetamine, J. Chromatogr. Sci. 26 (1988) 410–417.
[10] A.K. Valaer, W.R. Ravis, C.R. Clark, Liquid chromatographic properties and aqueous solution stability of *N*-hydroxy-3,4-methylenedioxyamphetmaine, J. Chromatogr. Sci. 28 (1990) 482–486.
[11] W.R. Ravis, A.K. Valaer, D. Brzozowski, C.R. Clark, The pharmacokinetics and liver metabolism of N-hydroxy-3,4-methylenedioxyamphetmaine (*N*-OH MDA) in rats, Life Sci. 54 (26) (1994) PL519–PL524.
[12] R. Kikura, Y. Nakahara, T. Mieczkowski, F. Tagliaro, Hair analysis for Drug Abuse XV. Disposition of 3,4-methylenedioxymethamphetamine (MDMA) and its related compounds into rat hair and application to hair analysis for MDMA abuse, Forensic Sci. Int. 84 (1997) 165–177.
[13] M. Shimamine, K. Takahashi, Y. Nakahara, Studies on the identification of psychotropic substances. IX. Preparation and various analytical data of reference standard of new psychotropic substances, N-ethyl methylenedioxyamphetamine, N-hydroxy methylenedioxyamphetamine, mecloqualone, 4-methylaminorex, phendimetrazine and phenmetrazine, Eisei Shikenjo Hokoku 111 (1993) 66–74.
[14] Y. Nakahara, K. Takahashi, M. Shimamine, Y. Takeda, Hair analysis for Drug Abuse. I. Determination of methamphetamine and amphetamine in hair by stable isotope dilution gas chromatography/mass spectrometry method, J. Forensic Sci. 36 (1991) 70–78.
[15] Y. Nakahara, K. Takahashi, R. Kikura, Hair analysis for drugs of abuse. X. Effect of physicochemical properties of drugs on the incorporation rates into hair, Biol. Pharm. Bull. 18 (9) (1995) 1223–1227.
[16] Y. Nakahara, R. Kikura, Hair analysis for drugs of abuse. XIII. Effect of structural factors on incorporation of drugs into hair: the incorporation rates of amphetamine analogs, Arch. Toxicol. 70 (1996) 841–849.
[17] A.H. Beckett, S. Al-Sarraj, The mechanism of oxidation of amphetamine enantiomorphs by lever microsomal preparation from different spices, J. Pharm. Pharmacol. 24 (2) (1972) 174–176.
[18] N. Uchiyama, R. Kikura-Hanajiri, K. Fukuhara, Y. Goda, Decomposition mechanism of *N*-OH-MDMA and *N*-OH-MDA in alkali solution, in preparation.
[19] P. Kintz (Ed.), Analytical and Practical Aspect of Drug Testing in Hair, CRC Press, FL, 2006.
[20] R. Kikura, Y. Nakahara, Studies on mechanism of drug incorporation into hair, Kokuritsu Iyakuhin Shokuhin Eisei Kenkyusho Hokoku 116 (1998) 30–45.
[21] M.C. Dumasia, Indentification of some *N*-hydroxylated metabolites of (±)-3,4-methylenedioxymethamphetamine in horse urine by gas chromatography–mass spectrometry, Xenobiotica 33 (10) (2003) 1013–1025.